International Journal of Nanomedicine

Dovepress
Taylor & Francis Group

Open Access Full Text Article

ORIGINAL RESEARCH

Lung-Targeted Itraconazole Delivery Using PVA-Based Nano-in-Microparticles for Improved Treatment of Pulmonary Aspergillosis

Jin-Hyuk Jeong[1,*], Hee-Sung Lee[1,*], Jae-Cheol Choi[1], Ji-Hyun Kang[2], Dong-Wook Kim[3], Chan-Su Park[1], Chun-Woong Park[1]

[1]College of Pharmacy, Chungbuk National University, Cheongju, 28160, Republic of Korea; [2]School of Pharmacy, Institute of New Drug Development, and Respiratory Drug Development Research Institute, Jeonbuk National University, Jeonju, Republic of Korea; [3]College of Pharmacy, Wonkwang University, Iksan, 54538, Republic of Korea

*These authors contributed equally to this work

Correspondence: Chun-Woong Park, College of Pharmacy, Chungbuk National University, Cheongju, 28160, Republic of Korea, Tel +82 43 261 3330, Fax +82 43 268 2732, Email cwpark@cbnu.ac.kr; Chan-Su Park, College of Pharmacy, Chungbuk National University, Cheongju, 28160, Republic of Korea, Tel +82 10 5841 9359, Email cpark@cbnu.ac.kr

Purpose: Pulmonary aspergillosis (PA) presents a substantial therapeutic challenge, especially in immunocompromised patients, where conventional systemic treatments like oral and intravenous routes often result in limited efficacy and increased adverse effects. This study focuses on the development and evaluation of an inhalable itraconazole (ITZ) formulation within a nanoparticles-in-microparticles (NIM) system.

Methods: Polyvinyl alcohol 500 (PVA), used in varying concentrations, played a crucial role as a stabilizer in both the wet bead milling and spray drying processes, enhancing drug release and aerodynamic performance. The influence of PVA ratios on drug penetration into pulmonary mucus and interactions with pulmonary defense mechanisms were thoroughly investigated through in-vitro simulations.

Results: Pharmacokinetic analysis in *Sprague-Dawley* (SD) rats revealed enhanced distribution of ITZ-NIMs in pulmonary tissues and bronchoalveolar lavage fluid (BALF), representing a significant improvement in localized drug concentration. Efficacy against *Aspergillus fumigatus* was confirmed by a reduction in galactomannan levels, inhibition of fungal growth in lung tissues, and increased survival rates. Importantly, pulmonary delivery of ITZ significantly reduced hepatotoxicity markers, including alanine aminotransferase (ALT) and alkaline phosphatase (ALP), when compared to oral administration.

Conclusion: The incorporation of PVA in NIM technology demonstrated not only improved pulmonary targeting and drug release but also minimized systemic toxicity, highlighting the potential of nanoparticle-based inhalation systems in treating respiratory fungal infections like aspergillosis. These findings emphasize the pivotal role of PVA in the formulation, stability, and therapeutic efficacy of NIM-based drug delivery systems for pulmonary applications, advancing the use of nanoparticle technology in respiratory drug delivery.

Keywords: Polyvinyl alcohol 500, PVA, dry powder inhaler, DPI, nanoparticles-in-microparticles, NIM, itraconazole, ITZ, aspergillosis

Introduction

Pulmonary aspergillosis (PA) is an advanced state of *Aspergillus fumigatus* (*A. fumigatus*) colonization that occurs after the germination of conidia. PA is a common cause of morbidity and mortality among immunocompromised individuals. Over the past 20 years, the incidence of PA infections has increased dramatically. *A. fumigatus* conidia can survive outdoors for extended periods while suspended in the air.[1] The most common mode of transmission is inhalation. The lungs serve as the primary gateway for this pathogen, often marking the initiation point for invasive entry, which can lead to fatal outcomes in more than 90% of cases.[2]

Received: 9 December 2024
Accepted: 31 March 2025
Published: 8 April 2025

Graphical Abstract

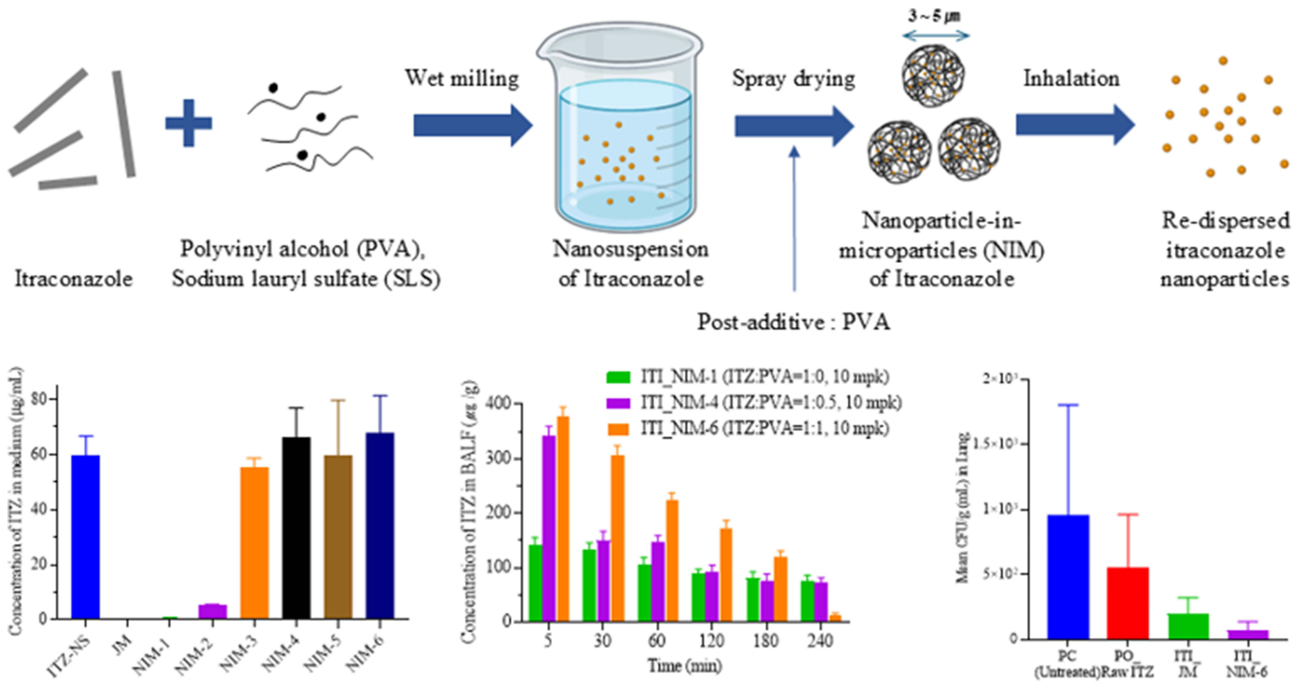

Despite the advancements in therapy, mortality rates remain exceedingly high once an invasive stage is reached. The disease progression in most immunocompromised patients is notably rapid.[1] The high treatment failure rate can be attributed to several factors. First, PA is difficult to diagnose in the early stages because of its non-specific symptoms. Often, by the time the first clinical symptoms appear (eg, hemoptysis), an invasive state has already been reached. Another critical reason for treatment failure is that the existing oral or intravenous administration methods require high systemic concentrations to achieve effective pulmonary levels, leading to numerous adverse effects and metabolic interactions.[3,4]

Itraconazole (ITZ) is widely regarded as a first-line drug for the treatment of aspergillosis.[5] Despite its extensive antifungal activity and high efficacy, ITZ has low solubility and can induce numerous side effects, including hepatotoxicity and metabolic interactions.[6,7] Additionally, the currently available forms of ITZ administered either intravenously or orally require high doses to ensure effective drug delivery to lung tissues and lesion sites.[8,9] Therefore, the pulmonary delivery of ITZ is a promising alternative to PA treatment. Specifically, *A. fumigatus* can become embedded within the mucous layers and remain in the pulmonary cavities. The delivery of ITZ through the lungs not only facilitates its delivery to pulmonary tissues, but also enables direct access to pathogens embedded within the pulmonary mucus.[10–12] Consequently, this delivery method is expected to enhance both the efficacy and safety of treatment.

Among pulmonary drug delivery formulations, dry powder inhalers (DPIs) are the most traditional and continue to be extensively developed.[13] Unlike liquid formulations, they offer chemical stability, do not require propellants,[14] and have a lower risk of formulation issues.[15] They are generally suitable for delivering high drug concentrations and ensure reproducibility and reliability.[16,17] To reach deeper lung penetration, it is essential for the drug particles in DPIs to have aerodynamic diameters ranging from 0.5 µm to 5 µm.[18] However, these fine powders often exhibit high cohesiveness, which leads to poor flowability.[19] Additionally, poorly soluble ITZ has the potential to dissolve slowly and incompletely in the lungs.[7] Undissolved ITZ particles can be eliminated through mucociliary clearance or macrophages.[20]

Nanoparticles are advantageous formulations for Class 2 and 4 drugs according to the Biopharmaceutics Classification System (BCS), where the dissolution rate is the rate-limiting step for absorption.[21] The rate of drug dissolution is inversely proportional to the particle diameter; therefore, reducing the particle size can enhance the dissolution rate. In addition, nanoparticles are effective in overcoming biological barriers.[22] Under conditions involving pulmonary administration, the lung mucus and bacterial biofilms present substantial barriers to drug penetration.[23] Drugs typically exhibit low diffusion rates and are susceptible to inactivation within mucosal layers or biological films. Depending on their physicochemical properties, nanoparticles possess the capability to penetrate these mucosal barriers and biofilms, facilitating more effective drug delivery.[24,25] Although nanoparticles have the potential to improve lung treatment, delivering them to the lungs is challenging. Particles between 0.1 and 1 μm exhibit low deposition efficiency upon inhalation.[26,27] Due to their high surface area-to-volume ratio, nanoparticles tend to form large agglomerates (>5 μm) that deposit in the upper airways through impaction.[28] Furthermore, inhaled non-agglomerated nanoparticles are likely to be expelled during exhalation. For nanoparticles to be successfully delivered to the lungs via inhalation, they must be transformed into inhalable microparticles while preserving their essential characteristics of the nanoparticles.

Therefore, DPI formulations require extensive particle-level engineering to balance interparticle forces in the dry powder bulk, ensuring sufficient stability during processing and storage as well as optimal dispersion and fine particle generation during inhalation[29] Among these techniques, spray drying is used to produce drugs and excipient particles that can be inhaled without further modification because of their excellent dispersibility and small mass median aerodynamic diameter (MMAD).[30] The component distribution within the spray-dried particles depends on the surface activity and diffusion characteristics of the sprayed droplet components, as well as the drying parameters. This also influences the particle size and shape and is used to control the production of materials with desired properties.[31] Typical spray-dried materials are low-density, somewhat spherical, amorphous particles.[32] Porous particles with low interparticle interactions can be formed by designing a process to promote early envelope formation and coating with hydrophobic surfactants. Despite their small size, these particles can be easily handled owing to their low cohesiveness. The best commercial example of this strategy is the PulmoSphere™ technology.[33]

Nevertheless, existing technologies such as PulmoSphere™ focus on delivering microparticles to the lungs. To preserve the drug's efficacy in the lungs, it may be advantageous to retain the unique properties of the nanoparticles. To overcome these limitations, a multistage formulation process known as Nanoparticles-in-Microparticles (NIM) technology has been proposed. This involves the preparation of nanoparticles and their incorporation into microparticles. NIM, also referred to as Trojan microparticles, facilitate stable storage and transportation of microparticles to the lungs. Upon reaching the lungs or a specific target site, these microparticles release nanoparticles that are capable of penetrating barriers.[34,35]

Another critical factor in facilitating this drug delivery process is the choice of material. Significant research has been conducted to develop controlled release formulations for pulmonary delivery, where the drug is encapsulated within polymers, copolymers, or lipids.[36,37] Among these materials, PVA stands out as a biocompatible and non-cytotoxic excipient.[38,39] PVA plays a crucial role in stabilizing nanoparticles or microparticles, thereby helping to maintain the structural integrity of the delivery system.[40] Additionally, PVA's hydrophilic nature supports efficient mucosal adhesion, allowing the drug to remain at the delivery site for a longer duration, and enhances interactions with the pulmonary mucus layer.[41,42] This improved retention and interaction can potentially enhance therapeutic efficacy in pulmonary drug delivery systems.[43]

Therefore, the objective of this study was to prepare ITZ-containing NIM formulations using spray drying, evaluate their efficacy against PA, and develop a DPI formulation that could potentially offer improved therapeutic effects and safety compared to oral administration. To enhance the stability and performance of the formulation, PVA was selected as a key excipient due to its biocompatibility and ability to stabilize nanoparticles. The inclusion of PVA in the NIM formulations was expected to (i) improve the aerodynamic performance of the spray-dried microparticles; (ii) facilitate more effective drug delivery to the lung cavities, pulmonary mucus, and pulmonary tissues by maintaining nanoparticle stability and promoting longer retention at the site of action; and (iii) ultimately lead to enhanced therapeutic outcomes for PA. This approach underscores the promising potential of combining ITZ with PVA in NIM formulations, offering a more efficient and targeted pulmonary treatment strategy for PA.

Materials and Methods

Materials

Itraconazole (ITZ) was purchased from SMS Pharmaceuticals Ltd. (India). Polyvinyl alcohol 500 (MW 22,000) was purchased from the OCI Company Co., Ltd. (Republic of Korea). Sodium lauryl sulfate (SLS) was purchased from DUKSAN Co. Ltd. (Republic of Korea). The water was purified by filtration in a laboratory. High-performance liquid chromatography (HPLC)-grade solvents were used for the analysis. HPLC-grade ethanol and acetonitrile (ACN) were purchased from Honeywell Burdick & Jackson (USA). All reagents were of analytical grade and were used without further purification.

Preparation Method

A two-step protocol was employed to prepare the NIMs. Initially, a nanosuspension (NS) was prepared using wet milling techniques with PVA, SLS, and ITZ. After dilution with PVA, the suspension was processed via co-spray drying to obtain the final micronized powder. Subsequently, the NIMs were prepared by varying the concentration of PVA and spray-drying the micronized powder. To facilitate a comparative analysis of the physicochemical properties and, in-vitro and in-vivo studies (pharmacokinetics and pharmacodynamics), jet-milled ITZ microparticles containing nanoparticles were prepared.

Preparation of Nanoparticles Using Wet Milling

PVA (225 mg) and SLS (23 mg) were dissolved in purified water to a final volume of 15 mL. Additionally, 75 g of ZrO_2 beads was employed as the milling medium in a planetary ball mill (Retsch Planetary Ball Mill PM 100 MA, Retsch GmbH, Germany).[44] The milling parameters were as follows: 120 min at 400 rpm with a bead size of 0.1 mm. This process resulted in NS containing ITZ, PVA, and SLS. The resulting ITZ-NS was diluted with purified water to a final volume of 500 mL to achieve an ITZ concentration of 6.25 g/L (Table 1).

Preparation of Nanoparticle-in-Microparticles Using Spray Drying

Different compositions were prepared by adding varying amounts of PVA (Table 1). The different formulations for spray drying were designated as ITZ: post-additive PVA ratios of 1:0, 1:0.1, 1:0.3, 1:0.5, 1:0.7, and 1:1. The ITZ was spray-dried using a laboratory scale spray dryer (EYELA SD-1000, Tokyo Rikakikai Co., Ltd., Japan) with the following parameters: inlet temperature of 160°C; outlet temperature of 85°C – 95°C; nozzle size of 0.7 mm, feeding rate of 1.7 mL/min; atomization air pressure of 150 kPa, and blower rate of 0.30 m3/min. The spray-dried ITZ nanoparticles-in-microparticles (ITZ-NIM) were kept in a glass vial containing silica gel at −20°C until used.[45]

Jet-Milling

The jet-milled ITZ microparticles (JM) were prepared using an air jet mill (A-O JET MILL, J S Tech Co., Ltd., Republic of Korea) with the following parameters: G nozzle: 0.5 MPa; P nozzle: 0.5 MPa. Nitrogen air was used for milling, and the JM were then kept in a glass vial containing silica gel at −20°C until used.

Table 1 Formulation of Itraconazole (ITZ) Nanoparticles-in-Microparticles (NIM)

No.	Nano Suspension (NS)			Dilution	Post-Additive	Total	(ITZ: Post-Additive PVA) Ratio
	ITZ (g)	PVA 500 (g)	SLS (g)	Water (mL)	PVA 500		
NIM-1	3.125	0.225	0.023	500	0	3.373	1:0
NIM-2	3.125	0.225	0.023	500	0.313	3.686	1:0.1
NIM-3	3.125	0.225	0.023	500	0.938	4.311	1:0.3
NIM-4	3.125	0.225	0.023	500	1.563	4.936	1:0.5
NIM-5	3.125	0.225	0.023	500	2.188	5.561	1:0.7
NIM-6	3.125	0.225	0.023	500	3.125	6.498	1:1

Physicochemical Properties of Nanoparticle-in-Microparticles

Scanning Electron Microscope (SEM)

JM and ITZ-NIM were visually imaged using a scanning electron microscope (SEM; ZEISS-GEMINI LEO 1530; Zeiss, Germany). The samples were placed onto carbon tape and were then coated with platinum using a Hummer VI sputtering device, reaching 200 Å coating thickness. A voltage of 3 kV and magnifications of 3,000 × and 10,000 × were used.

Transmission Electron Microscope (TEM)

The electron beam emitted from the high voltage passed through the ultrathin sample to form a two-dimensional image according to the electron density, allowing observation of the ultrafine structure inside the sample. After transferring the ITZ-NS and ITZ-NIM samples to a copper grid, negative staining was performed using 1% phosphotungstic acid, and the samples were completely dried for 2 h at 40°C in a dry oven. The images were captured at a magnification of 15,000× under an accelerating voltage of 120 kV.

Particle Size Distribution (PSD)

The particle size distribution of the NSs were determined using a dynamic light scattering technique (DLS, Litesizer 500, Anton paar, AT, measurement range of 0.3 nm – 10.0 µm). One milliliter of each sample was added to 50 mL of distilled water, and the suspensions were vortexed for 20s and allowed to equilibrate for 1 h. The measured mean particle size and size distribution were expressed as the Z-average and polydispersity index (PDI). The particle size distribution of the nanoparticle-in-microparticles was determined by laser diffraction (Malvern Mastersizer Scirocco 2000, Malvern Instruments Ltd., UK). A dry dispersion unit was used to observe the spray-dried nanoparticle-in-microparticles. Approximately 1.0–2.0 g of the product was loaded onto a feeding tray. The air pressure was adjusted to 3.0 bar and 25% vibration feed was used. Each sample was measured in triplicate.

Differential Scanning Calorimetry (DSC)

DSC was performed using a Q2000 instrument (TA Instruments Ltd., USA). ITZ, JM, and NIM 1–6 weighing approximately 1 mg, were placed in aluminum pans and sealed hermetically. The samples were heated 0°C – 250°C at a heating rate of 10°C/min. All experiments were conducted in triplicates.

Powder X-Ray Diffraction (PXRD)

PXRD patterns were obtained using an X'Pert PRO MRD® (PANAlytical Ltd., Netherlands) with Cu K radiation at 50 mA and 40 kV. The nanoparticle-in-microparticles (JM, NIM 1–6) were placed on plates at room temperature. 2θ scans were collected from 5° to 60°.

Fourier Transform Infrared (FT-IR)

FT-IR was performed on raw ITZ, JM, and NIM 1–6 in the range of 500–4000 cm^{-1}, using IFS 66/S® (BRUKER OPTIK GMBH Ltd., USA).

In-Vitro Aerodynamic Performance

In accordance with the USP Chapter <601> specifications for aerosols, the aerodynamic performance of the ITZ-NIM 1–6 formulations were evaluated using a next-generation impactor (NGI, Copley Scientific Limited., Nottingham, UK) and RS01® DPI device. To prevent particle bounce and re-entrainment, the collection plates of the NGI stages were pre-coated with 3% silicone oil in hexane. Each sample, containing 10 mg of the ITZ-NIM DPIs formulation, was loaded into hydroxypropyl methylcellulose hard capsules (size 3). A capsule was inserted into the RS-01, and the device was inserted into the mouthpiece of the induction port. Air was inhaled at a controlled flow rate of 60 L/min for 4 s. For an NGI flow rate of 60 L/min, the aerodynamic cutoff diameters of each stage were determined as 8.06 µm, 4.46 µm, 2.82 µm, 1.66 µm, 0.94 µm, 0.55 µm, 0.34 µm, and 0.14 µm for stages 1–7 and Micro Orifice Collector (MOC). The quantity of sample remaining in the capsule and deposited on each collection plate at each stage was quantified using HPLC. The parameters of the aerosolization performance were calculated by Inhalytix® software (Copley Scientific Ltd., Nottingham, UK), ie, fine particle fraction (FPF), fine particle dose (FPD), mass median aerodynamic diameter (MMAD), and geometric standard deviation (GSD).

Example of Equation:

Emitted Dose [ED, %] = [(Initial Mass in Capsule − Final Mass Remaining in Capsule)/(Initial Mass in Capsule)]

Fine Particle Fraction [FPF, %] = [Mass of Particles in Stages 2-MOC]/[Mass of Particles in All Stages].

The mass median aerodynamic diameter (MMAD) and geometric standard deviation (GSD) were calculated using the guidelines provided in USP Chapter 601. The MMAD was determined from a plot of a mass fraction smaller than the aerodynamic diameter, specified as D50%, on a logarithmic probability scale. The GSD was calculated using the following equation:

GSD = √[D84.13%/D15.87%].

In-vitro Behavior of NIMs in Artificial Mucus (AM) Layer

Diffusion across the artificial mucus (AM) layer into the lung fluid was demonstrated using simulated lung fluid (SLF) prepared according to literature protocols.[46] In brief, the SLF was prepared according to the recipe described in Table S1, and the pH of the fluid was maintained between 7.0 and 7.2 throughout the experiment. Using Franz diffusion cell apparatus (Phoenix DB-6, Teledyne Hanson Research, Inc., USA), a formulation containing 1 mg of itraconazole was loaded onto a regenerated cellulose (RC) membrane using a dry powder insufflator (DP-4, Penn-Century Inc., USA), and 15 mL of SLF was added to the receptor phase of the Franz diffusion cell, maintained at 37°C for 30 minutes under stirring at 150 rpm. Subsequently, the particle morphologies of the RC membranes were examined by SEM. The particle size and PDI of the receptor were measured after 100-fold dilution with water. The ITZ concentration in the dispersion was quantitatively analyzed using high-performance liquid chromatography (HPLC). PVA was dissolved in water, the particle size (excluding the drugs) was measured, and the particles were found to consist only of nanoparticles. The re-dispersed fraction of nanoparticles was calculated by relating the nanoparticles in the dispersion to the theoretical nanoparticle content.

Additionally, the upper well of a 24-transwell system was utilized to simulate the mucosal surface and mucus layer, with the mucus layer thickness set at 50 μm to reflect a patient's condition. The receptor phase, containing 12 mL of SLF, was used to model epithelial cells separated by a semipermeable film with a pore size of 0.4 μm. The effective diffusion area is 0.33 cm^2. The stirring bar rotation was maintained at 400 rpm, and the temperature was kept constant at 37°C. The ITZ content of each formulation was measured to be 1.5 mg, and the formulation was incubated for 4 h. The ITZ concentrations at the apical, artificial mucus, and basal surfaces were measured using HPLC at the end of the incubation period.

Macrophage Uptake Study

To evaluate the ability of ITZ-NIM to resist uptake by lung-resident macrophages, mouse macrophages (RAW 264.7 cells, ATCC) were seeded in a 24-well plate at a density of 5×10^5 cells/well. ITZ-NS, JM or ITZ-NIM were reconstituted in RPMI-1640 cell culture medium at a final ITZ concentration of 100 μM. Each well was then treated with 1 mL of the suspension and incubated for 2 h. Subsequently, the cells were detached using cell scrapers and collected by centrifugation at 1,500 × g for 10 min. The cells were lyophilized overnight. Subsequently, 1 mL of methanol was added to each sample and incubation was continued overnight to extract the drug. The supernatant was completely suctioned and analyzed quantitatively. The drug content in both the cell pellet and supernatant was measured; the drug extracted from the cell indicated phagocytosis by macrophages, whereas the drug in the supernatant was considered a drug that was not phagocytized by macrophages.

In-vivo Pharmacokinetic and Pharmacodynamics Studies in SD Rats

Animal and Experimental Design

This animal care and use protocol was reviewed and approval by the IACUC as Chungbuk National University (Republic of Korea, Approval number: CBNUA-24-0019-03).

Sprague Dawley (SD) rats (male, 250–300 g) were purchased from SAMTAKO BIO KOREA (Republic of Korea) and provided ad libitum. SD rats were divided into five groups (n = 5) and treated with 10 mg/kg JM, NIM-4, or NIM-6 using the method described below. The oral formulation was suspended and loaded into a syringe equipped with a zone. The DPI formulations (JM, NIM-4, and NIM-6) were loaded into a DP-4R dry powder insufflator equipped with an SC-X sample chamber expander (Penn-Century Inc., USA). To conduct pharmacokinetics study, the rats were anaesthetized with isoflurane, and 500 µL of blood was taken from the eyeground veins. (Timepoint: 0.5, 1, 2, 4, 6, 8, 12, 24 h). Blood samples were stored in heparin-coated tubes immediately after collection. Plasma was obtained by centrifugation (15 min at 4,000 rpm). Plasma was analyzed as soon as it was obtained. Proteins in the plasma were precipitated using ACN. The ACN was added at 200 µL per 200 µL of plasma and left to stand for 30 minutes after mixing and centrifuged (10,000 rpm for 15 min). Aliquots (20 µL) of the supernatant were injected for HPLC analysis. After administration, four rats from each group were sacrificed at 5, 60, and 180 min at each time point to obtain the lungs. Plasma, lung tissue, and BALF were collected from the sacrificed SD rats. Subsequently, the lung tissues were homogenized, and the homogenates were subjected to solvent precipitation prior to analysis of the pharmaceutical compounds.[47]

Preparation of *A. Fumigatus*

A. fumigatus was purchased from ATCC (MYA-4609). The spores were cultivated on potato dextrose agar (PDA) plates. The spores were grown on PDA plates for 3–5 d at 28 °C and harvested, resuspended in phosphate buffer saline with 0.05% Tween 80 (PBS-T).[48]

In-vivo *A. Fumigatus* Infection

To select the immunosuppressive regimen, 50 mg/kg of cyclosporine A and 0.5 mg per kg of tacrolimus were administered by intraperitoneal injection.[49,50] It was administered thrice a week for two weeks. The *A. fumigatus* strain (1×10^8 spores/200 µL/rat) was administered by intratracheal installation (ITI).[51,52] Passing through the upper airways, the MicroSprayer® Aerosolizer device was proven to generate an air-dispersed controlled cloud of conidia in the bronchial-tracheal apparatus of rats, mimicking the real pathophysiology of airborne *A. fumigatus* exposure.[53] The rats were divided into five experimental groups (n=4): no *A. fumigatus* infection group (NC), untreated control group (PC), group treated with raw ITZ at 10 mg/kg orally (PO_Raw ITZ), group treated with ITZ via intratracheal administration of the JM formulation (ITI_JM), and group treated with ITZ via intratracheal administration of the NIM-6 formulation (ITI_NIM-6). Treatment was performed daily for two weeks. After the experimental infection, the body weight and survival rate of the SD rats were measured daily. The SD rats reduced to less than 20% body weight and sacrificed to obtain plasma, lungs, and BALF.[48,54]

Galactomannan (GM) Antigen Enzyme-Linked Immunosorbent Assay (ELISA)

GM in rat serum was measured using a General GM antigen ELISA kit (MyBioSource, USA) according to the manufacturer's instructions. Briefly, the serum samples were added to an ELISA plate and incubated for 30 min at RT. The HRP-conjugated reagent was then added to the plate and incubated for 1 h at RT. The reactions were developed 50 µL of Chromogen Solution A and 50 µL of Chromogen B and terminated by adding 50 µL of 2 mm H2SO4. The plate was then read with a microplate reader at an absorbance of 450 nm.[55,56]

Serum Assessments for Hepatotoxicity

Liver enzyme activity is often measured to assess the liver health and function. The two most measured liver enzymes are Alanine Aminotransferase (ALT) and Alkaline Phosphatase (ALP). ALT and ALP levels were determined using an automatic blood biochemical analyzer (Model 7180; Hitachi High-Technologies Corp., Tokyo, Japan).[57]

Tissue Isolation and Fungal Burden Assessment

The rats were divided into five groups (n=4 per group) and their weights and survival rates were measured daily. The rats were euthanized, and serum and BALF were collected. The rats were then quickly dissected, and the lungs were quickly harvested for use in subsequent experiments. Left lungs were preserved in 10% formalin overnight at 4 °C. Paraffin-embedded sections were stained with hematoxylin and eosin (H&E) and visualized under an optical microscope (LEICA, DM 2500, Germany). Stained tissue samples were magnified 40× to obtain microscopic images of the primary bronchus and alveolar.[58] The right lung was removed from the body, crushed with steel beads, and immersed in 2 mL of PBS-T. Homogeneous tissue samples were cultured for 3 d at 28°C by serial dilution with PBS-T and repeatedly incubating them on PDA plates. The number of colony-forming units (CFU) was measured after 3 d of cultured.[59]

High Performance Liquid Chromatography (HPLC) -UV Analytical Method

The HPLC method for quantitative analysis of ITZ was conducted using a Thermo Ultimate 3000 hPLC system (Thermo Scientific, Waltham, Middlesex County, USA). The column was an Inertsil ODS-2250×4.6 mm, 5 µm HPLC analytical column (GL Sciences, Japan). The mobile phase was composed of a mixture of a buffer containing 27.2 mg of tetrabutylammonium hydrogen sulfate dissolved in 1,000 mL of water and ACN in a ratio of 30:70 (v/v). The mobile phase was filtered through a 0.45 µm membrane filter (Whatman, UK) and then degassed before use. The mobile phase was pumped through the column at a flow rate of 2.0 mL/min. The column temperature was set to 30 °C, and the detection wavelength was 225 nm. The injected volume of each sample was 20 µL. The HPLC retention time was 10 min, and ITZ was detected at 6.0 min.

The standard curve was obtained at eight points (100, 50, 25, 12.5, 6.25, 3.13, 1.56, and 0.78 µg/mL) based on dilutions of the standard ITZ solution at 100 µg/mL. The correlation coefficient of the standard curve was 0.99999. The limit of detection (LOD) and the limit of quantification (LOQ) were calculated using the standard deviation method and were determined to be 0.59 µg/mL and 1.78 µg/mL, respectively. The HPLC method was validated for the calculations.

Statistics

Statistically significant differences in physicochemical properties, in-vitro studies, and in-vivo studies (pharmacokinetics and pharmacodynamics) were evaluated using one-way analysis of variance (ANOVA) and Tukey's / Dunnett's post hoc test (SPSS version 23, SPSS Inc., USA). Statistical significance was set at $p < 0.05$.

Results and Discussion

Physicochemical Properties of Nanoparticle-in-Microparticles

Morphology

The morphologies of the samples are shown in Figure 1. Additionally, the physicochemical properties of the particles, such as the true density and zeta potential, are presented in Table S2. Figure 1A and C-Hare SEM images, whereas panel Figure 1B displays a TEM image of ITZ-NS. The raw ITZ exhibited needle-shaped particles, which were thin and elongated, measuring tens of micrometers in size. Conversely, the ITZ-NS produced through wet ball milling predominantly exhibited irregular shapes smaller than 500 nm. In NIM-1, which did not incorporate PVA during spray drying, the milled ITZ particles exhibited aggregated forms. From NIM-2 onwards, when PVA was added during the spray drying process, the surfaces became progressively smoother as more PVA was incorporated.[60] However, NIM-2, an intermediate stage, had a surface with filled gaps and aggregated forms, creating a rough texture with pores. NIM-3, where the PVA/ITZ ratio reached 1:0.3, showed almost no fine pores but retained a rough surface. In NIM-4, the surface smoothened and larger undulations in the particles were emphasized. This trend continued for NIM-5 and NIM-6, where an increase in the PVA content resulted in smoother surfaces and deeper undulations in the particle structure. NIM-6 displayed such severe shrinkage that the innermost folds of the particle undulations were not visible. These morphological features align with the Reynolds theory, suggesting that an increase in the viscosity of the hydrophilic substrate PVA reduces solute diffusion during spray drying, causing the particles to fold more significantly and indent.[61] While the overall size of the manufactured NIM particles remained similar, the smoothness or roughness of the surface and the degree of particle undulation significantly affected the aerodynamic performance. Previous studies have suggested that rough or porous surfaces can enhance particle adhesion.[62] Furthermore, small undulations such as dimples can improve the aerodynamic inhalation efficiency, whereas larger macroscale undulations may cause interlocking among particles, thereby reducing the inhalation efficiency.

Particle Size Distribution (PSD) by Laser Diffraction

The particle size distributions of the formulations are summarized in Figure 2A. The NSs were prepared using raw ITZ and PVA during milling. In the final ITZ-NS formulation (Table S3), the particle size of ITZ was 270 nm ± 5 nm, with a PDI of 0.17 ± 0.02. Following spray drying, all formulations had a Dv50 value within the range of 1–5 µm with monodisperse distribution, making the particle size suitable for pulmonary delivery. The incorporation of PVA into the formulation increased the geometric size of the spray-dried particles. The distribution was monodispersed in all cases (span < 2.0), which was essential for accurate dosing.[63,64] To avoid mucociliary clearance and macrophage uptake during the

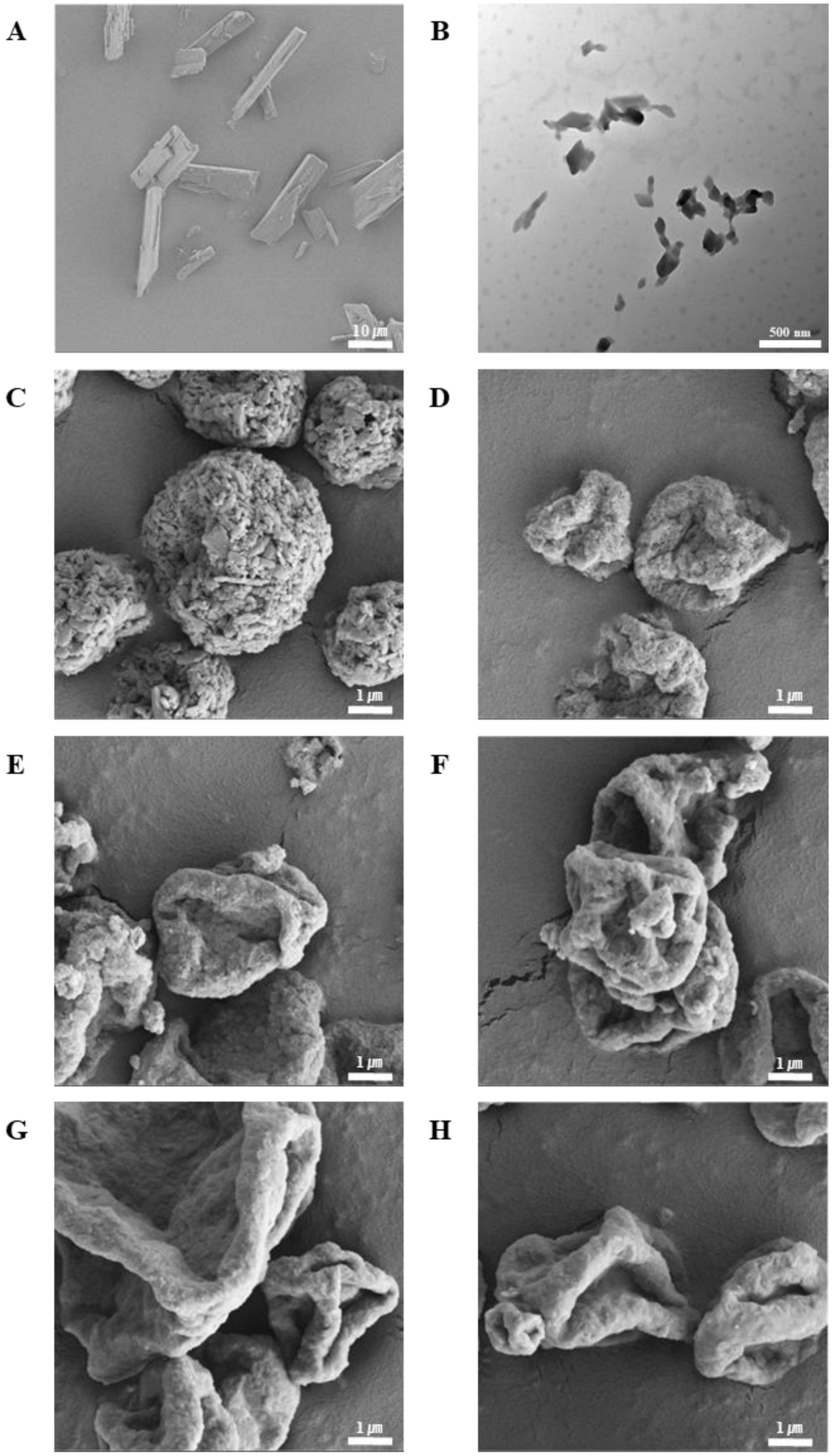

Figure 1 SEM image and TEM image of ITZ particle; (**A**) SEM image of Raw ITZ, (**B**) TEM image of ITZ-NS, (**C** - **H**) SEM image of ITZ NIM-1 to NIM-6, respectively.

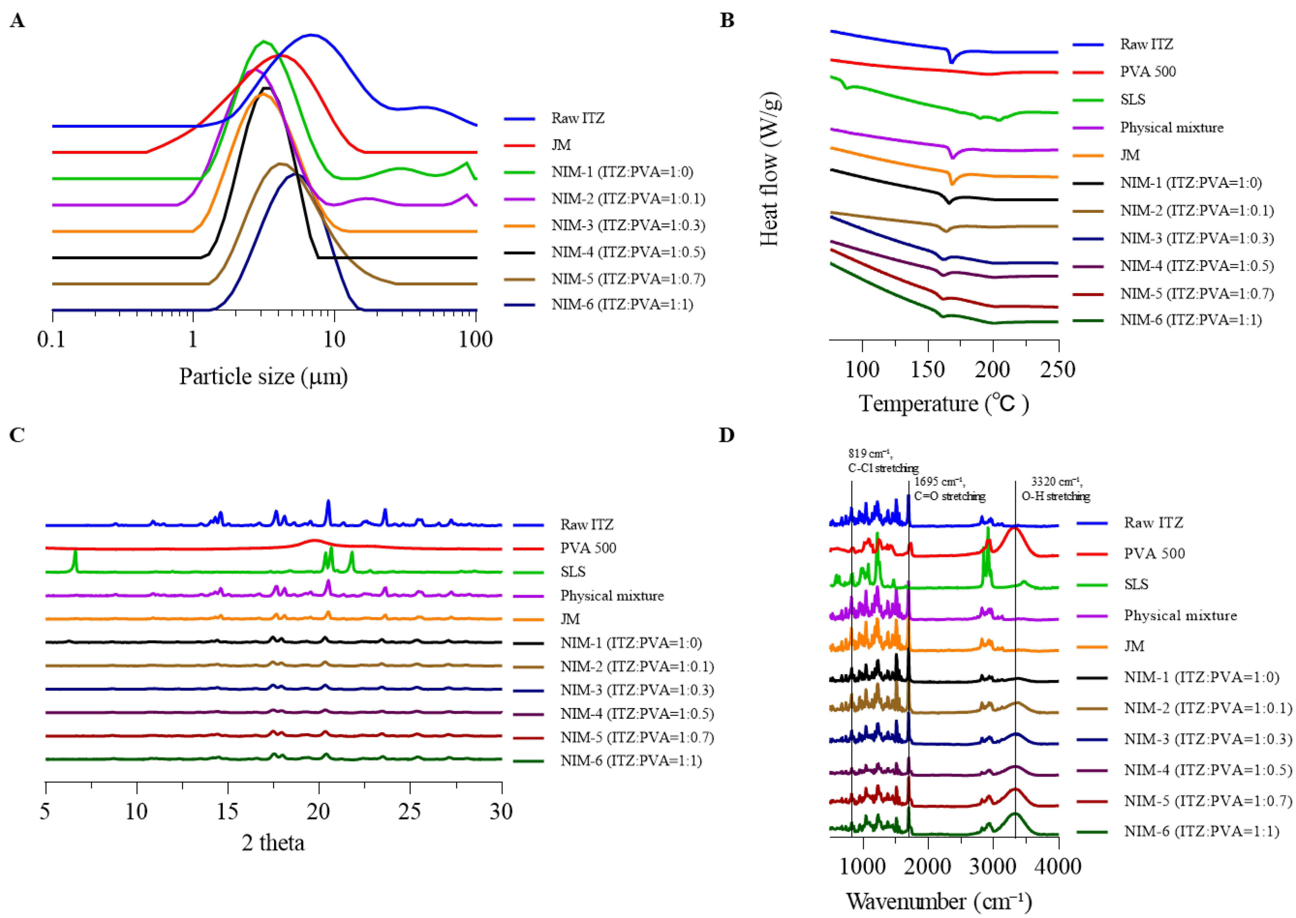

Figure 2 Physicochemical characteristics of NIMs; (**A**) PSD using laser diffraction, (**B**) DSC thermograms, (**C**) PXRD patterns, (**D**) FT-IR spectra.

determination of nano particle size, the Dv90 value (µm) was set below 0.3 µm (Figure S1). PDI typically allows monodispersed below 1, with a criterion set below 0.2 to producing more uniform particles.[65] The MMAD may vary depending on particle density or shape. Nonetheless, particles larger than 5 µm generally cannot follow the airflow direction changes at the upper and branching airway bifurcations due to inertial impaction. Particles smaller than 1 µm are typically exhaled. Ultimately, the required particle size range for pulmonary therapy falls within a diameter of 1–5 µm.[66]

Crystallinity

The crystal state was determined by DSC and PXRD. In the thermal analysis depicted in Figure 2B, DSC was employed to evaluate the impact of excipients and processing conditions on the physical properties of the ITZ. PVA exhibited no endothermic peaks during DSC analysis.[67] The DSC thermograms of raw ITZ displayed a pronounced endothermic peak at 167.4°C, indicative of its melting point and crystalline nature.[68,69] Following milling and spray drying, the DSC thermograms consistently showed broader endothermic peaks for ITZ, suggesting a reduction in drug crystallinity. The decrease in the melting temperature of the residual ITZ crystals in the formulations relative to those in the raw ITZ can be attributed to the reduced particle size and increased amorphization facilitated by PVA. Comparison with the PXRD data revealed no alterations in the crystal state (Figure 2C), including no shifts or deformations in the crystal structure. Although there were no changes in the molecular structure or crystallinity of the compound, the addition of PVA diminished the agglomeration energy of the particles, thereby lowering the melting point of the ITZ. During the spray drying process employed in the manufacture of NIM, the melting point of the drug is reduced, yet the molecular structure and crystallinity remain unaltered.

As illustrated in Figure 2C, the PXRD patterns were used to characterize the crystalline state of the ITZ after preparation. The XRD patterns of the raw materials confirm the crystalline structure of the ITZ, as anticipated.

Specifically, raw ITZ exhibited characteristic diffraction peaks with the highest intensities at 8.9°, 10.9°, 14.5°, 17.5°, 20.5°, 23.6°, 25.5°, and 27.2° 2-theta, indicative of its crystalline nature.[68,70] However, in the formulations, the intensities of these characteristic peaks were diminished. The incorporation of PVA and SLS had no discernible influence on the diffractograms. Throughout the milling and spray-drying processes, a notable reduction in crystallinity was apparent. This reduction was quantified by measuring the decrease in the total area under the curve of the characteristic peaks relative to those of the physical mixtures.[71]

Fourier Transform Infrared (FT-IR)

The FT-IR spectrum of the raw ITZ is shown in Figure 2D. The predominant peaks of raw ITZ were identified at 3382, 3130, 3072, 2964, 2825, 1695, 1509, 1452, 734, and 673 cm^{-1}. The absorption bands ranging from 2800 cm^{-1} to 3200 cm^{-1} correspond to the stretching vibrations of C-H bonds, encompassing both alkane and aromatic types. Specifically, the band at 3382 cm^{-1} was attributed to the stretching vibration of the CH group in the furan ring, and the band at 734 cm^{-1} was associated with C-Cl stretching within the ITZ molecule. Additionally, the bands at 3130 and 3072 cm^{-1} are due to the stretching vibrations of the amino group. The pronounced band at 1695 cm^{-1} is indicative of C=O stretching, whereas the bands at 1509 and 1452 cm^{-1} correspond to the stretching vibrations of C=C and C-N bonds, respectively.[72]

In-Vitro Aerodynamic Performance Study

The aerodynamic parameters of the test tubes are listed in Table 2. The MMAD of the manufactured formulations ranged from 2.5 to 3.2 µm. The FPF values of the samples varied from 64.6% to 89.9%. The stagewise distribution of next-generation impactors is shown in Figure S2. The JM sample exhibited approximately 30% deposition in the induction port simulating the upper airways and showed lower FPF values (58.7%) and higher MMAD values (3.5 µm) compared to the NIM formulation. Among the NIM formulations, the lowest PVA concentration resulted in the highest FPF value (89.9%), as can be discussed similarly to the SEM images. The application of PVA influenced the surface characteristics of the particles, with higher PVA concentrations reducing the aerosolization of the product owing to particle agglomeration or folding.[73,74] Formulations with lower PVA concentrations achieved deeper deposition in the NGI, utilizing smaller MMAD (2.5 µm) and higher FPF (89.9%). In contrast, all NIM formulations exhibited high level of emitted dose percentages (ED%) (84.8–91.1%) and demonstrated superior FPF (64.6–89.9%). All the formulations exhibited uniform aerodynamic parameters. Compared with the JM formulations, the NIM formulations demonstrated even greater uniformity in their aerodynamic parameters. Minimal variations in ED and FPF are crucial to ensure the efficacy and safety of the designed medication. An important point of this study is that the results are consistent with the findings of the morphological study.[62,75,76] NIM-1 and NIM-2, which have pores and small undulations, exhibited very high inhalation efficiencies, with a FPF of over 85%. As the PVA ratio increased and the undulations became relatively large, FPF decreased slightly. However, all NIM formulations still demonstrated high inhalation efficiency, with an FPF of over 60%.

Table 2 Aerodynamic Performance Characteristics of JM and NIMs Including ED, FPF, MMAD and GSD (Mean ± SD, n=3)

Formulation	ED (%)	FPF (%)	MMAD (µm)	GSD
JM	87.1 ± 1.4	58.7 ± 2.3	3.5 ± 0.1	1.8 ± 0.1
NIM-1 (ITZ:PVA=1:0)	91.1 ± 0.1	89.9 ± 0.1	2.5 ± 0.1	1.8 ± 0.1
NIM-2 (ITZ:PVA=1:0.1)	87.4 ± 0.2	85.5 ± 0.1	2.6 ± 0.1	1.7 ± 0.1
NIM-3 (ITZ:PVA=1:0.3)	87.6 ± 0.3	76.6 ± 0.2	2.8 ± 0.1	1.8 ± 0.1
NIM-4 (ITZ:PVA=1:0.5)	86.2 ± 0.3	73.7 ± 0.2	2.9 ± 0.1	1.7 ± 0.1
NIM-5 (ITZ:PVA=1:0.7)	87.8 ± 0.1	70.1 ± 0.4	3.2 ± 0.1	1.8 ± 0.1
NIM-6 (ITZ:PVA=1:1)	84.8 ± 0.2	64.6 ± 0.3	3.1 ± 0.1	1.8 ± 0.1

https://doi.org/10.2147/IJN.S511099

In-Vitro Behavior of NIMs in Artificial Mucus (AM) Layer

Upon arrival of NIM in the lungs, its behavior within the mucus layer and its potential absorption into the body were simulated. This study aimed to confirm that the NIM formulation delivered nanoparticles to the lungs and verify their behavior an in-vitro. Figure 3 confirms the presence of particles on the Franz diffusion cell membrane initially and after 30 min, indicating the loading of NIM onto the membrane. Both NIM-1, without the post-addition of PVA, and NIM-2, with the post-addition of PVA at a ratio of 0.1 compared to ITZ, exhibited abundant microparticles on the membrane surface even after 30 min. In contrast, no microparticles were observed for NIM-4 or NIM-6. However, NIM-4 showed some signs of membrane surface alteration compared with NIM-6, although microparticles were not evident. As the PVA ratio increased, the hydrophilicity of the particles increased. Consequently, in NIM-1 and NIM-2, many particles remained intact on the membrane, whereas in NIM-6, the particles were almost completely disintegrated and penetrated, fully revealing the membrane structure. In NIM-4, the particles partially dissolved to the extent that their forms were not visible; however, they did not completely disintegrate. Instead, they appeared to cover the pores of the membrane in a suspended state.[77]

Figure 4 illustrates the characteristics of the permeated nanoparticles. The particles that penetrated the membrane exhibited a morphology like that of the initially prepared ITZ-NS, indicating that the drug remained undissolved and redistributed (Figure 4A). Although the initial nano particle shape and size were indiscernible in formulations with low PVA concentrations (NIM-1, 2), formulations with high PVA concentrations (NIM-4, 6) showed measurable size distributions like those of the initial nanoparticles (Figure 4A and C). Additionally, quantitative analysis of drug concentrations in the receptor phase revealed that formulations with higher PVA concentrations exhibited sequential disintegration of microparticles acting as carriers and drug permeation rates (Figure 4B). The increased ratio of PVA led to an increased disintegration rate of the NIMs with increased redispersion rates of the nanoparticles. The amount of the drug diffusing from the simulated pulmonary AM into the epithelium was measured (Figure 4D). When the PVA concentration of the NIM formulations changes, the extent to which nanoparticles of NIM diffuse into the AM differs.[78] The amount of ITZ on the apical side was measured in the following order: RAW ITZ, JM, NIM 1, 2, 4, 6 formulations, with concentrations of 47.4±6.5, 43.9 ±8.0, 48.4±28.3, 51.7±16.1, 13.5±2.0, and 16.1 ± 4.2 g/ mL, respectively. Substantial amounts of the drug were detected in formulations with poor disintegration (RAW ITZ, JM, and NIM 1 and 2), indicating that the drug in particulate form was not absorbed by the artificial mucosal barrier. Conversely, following RAW ITZ, JM, NIM 1, 2, 4, 6 formulations the amount of ITZ within the AM was measured at 8.3±5.2, 15.3±10.3, 2.8±0.7, 7.5±6.4, 43.7 ±6.7, 49.1±8.9 µg/mL, respectively. This suggests that the nanoparticles rapidly dissolved in the mucus layer due to the solubility of PVA.[79] This aspect is a crucial factor in the design of NIM. To maximize the advantages of microparticles during storage and inhalation, promote nanoparticle absorption upon reaching the lungs, and evade phagocytosis, it is essential for the nanoparticles to rapidly dissolve in the mucus layer, which serves as the first barrier encountered in the lungs.

Macrophage Uptake

After confirming the behavior of the nanoparticles within the mucosal layer, the resistance of the NIM formulations to phagocytosis by macrophages was evaluated in-vitro (Figure 5A). Additionally, quantification of ITZ in RAW 264.7, incubated in uninfected medium, is presented in Figure 5B. The amount of ITZ uptake by RAW 264.7 cells treated with ITZ-NS, NIM-3, NIM-4, NIM-5, and NIM-6 was negligible. In contrast, the intracellular ITZ concentrations of JM, NIM-1, and NIM-2 were 24.4 ± 1.0, 10.7 ± 0.8, and 6.2 ± 0.7 µg/mL, respectively. Furthermore, medium concentrations of ITZ reflected a trend opposite to that of the uptake by Raw264.7 cells. It is generally known that phagocytosis can be promoted by particle characteristics such as size and shape. The conditions that most enhance the uptake by representative alveolar macrophages include particles of 100–200 nm and 1–6 µm in size, spherical shape, hard and non-porous structure, and insoluble and hydrophobic properties.[80–82] Therefore, the high phagocytic activity of the JM particles may originate from their size, shape, and solubility. As the PVA content increased in the NIM formulations, nanoparticles were swiftly transported through the mucus

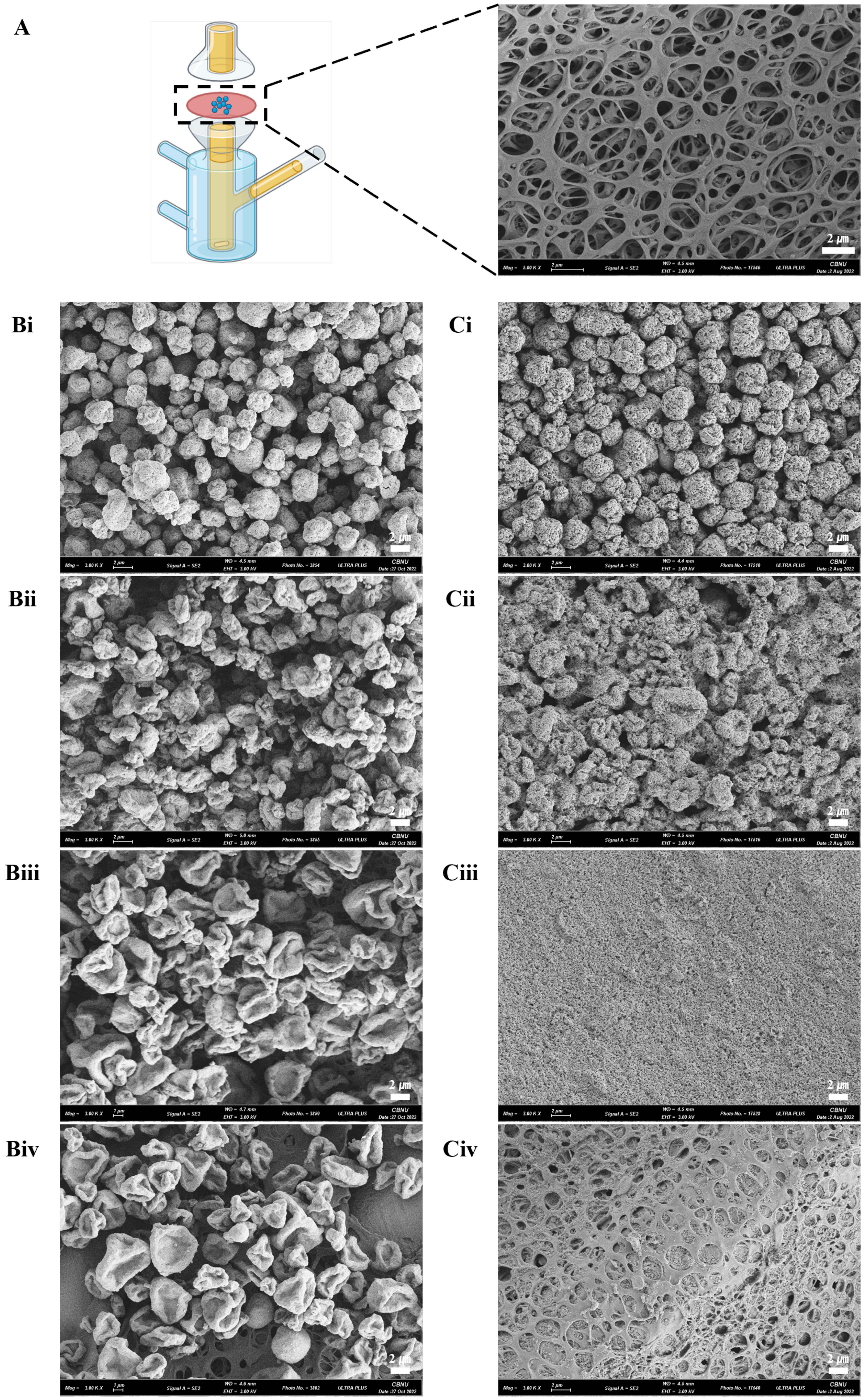

Figure 3 (**A**) Schematic diagram of the Franz diffusion cell apparatus and SEM image of the raw RC membrane (0.45 µm) at 5,000x magnification. SEM images of NIM loaded on the RC membrane of the AM layer over time, at 3,000x magnification.; (**B**) Membranes immediately after loading: (Bi) to (Biv) correspond to NIM-1, 2, 4, and 6, respectively. (**C**) Membranes 30 minutes after loading: (Ci) to (Civ) correspond to NIM-1, 2, 4, and 6, respectively. The schematic diagram of the Franz diffusion cell apparatus in (**A**) was created with BioRender.com.

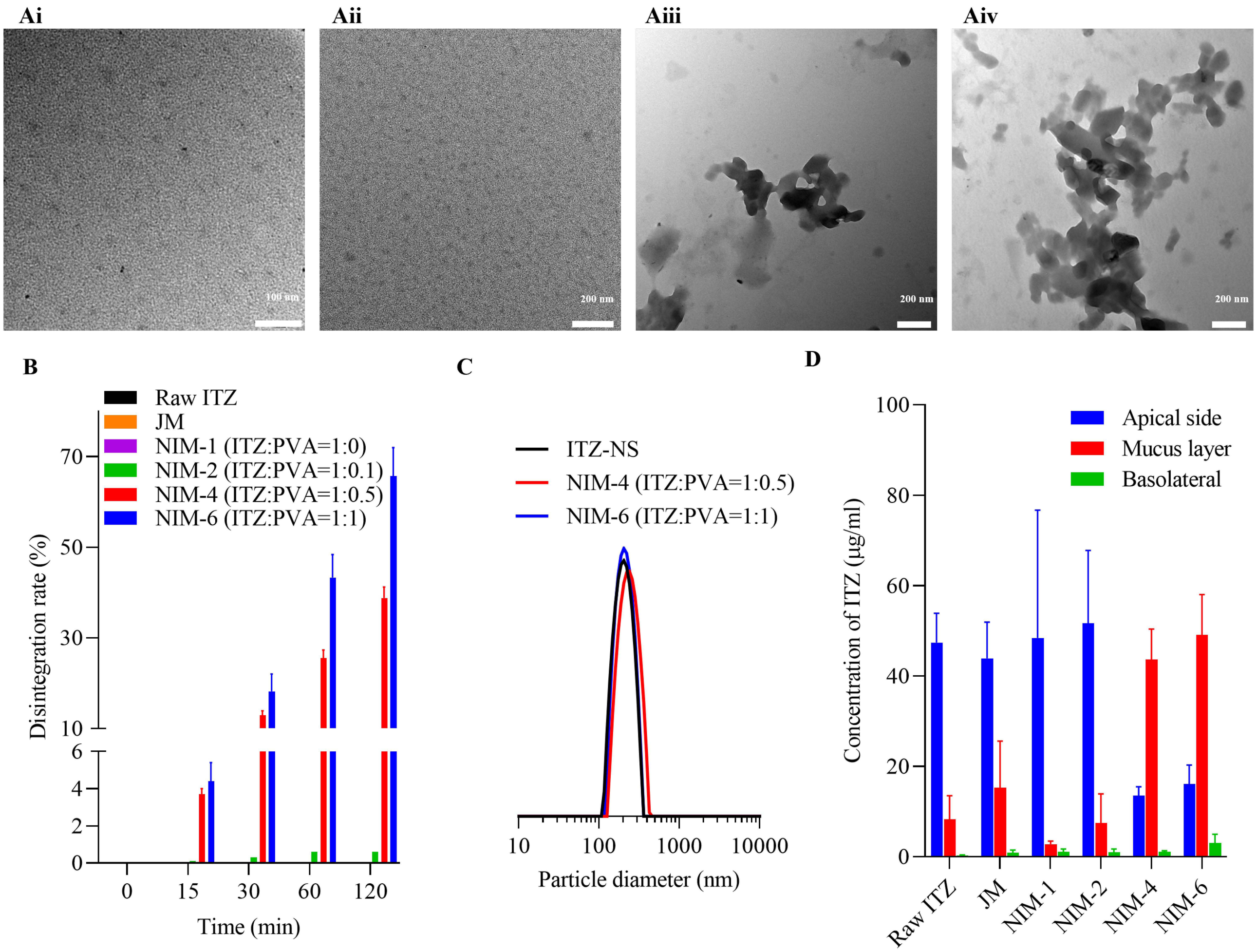

Figure 4 Evaluation of NIMs characteristics in the in-vitro artificial mucus (AM) layer: (**A**) TEM image of ITZ nanoparticles re-dispersed in the basal area; (Ai) to (Aiv) correspond to NIM-1 to NIM-4, respectively. (**B**) Time-dependent dissolution rate of NIMs calculated from the analysis of ITZ content re-dispersed in the basal area, (**C**) Particle size distribution (PSD) of particles re-dispersed in the basal area using Dynamic Light Scattering (DLS), (**D**) Distribution of NIM content in the Trans-well (mean ± SD, n=3). Statistical analysis in (**B**) was performed using a Two-way ANOVA with Tukey's multiple test with Raw ITZ.

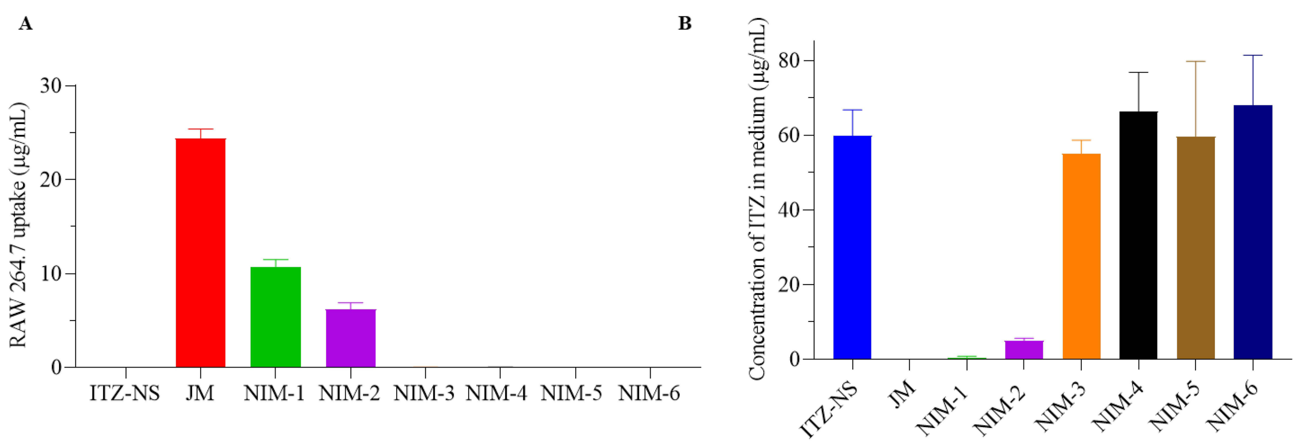

Figure 5 (**A**) Cellular uptake of ITZ by RAW 264.7 cells, (**B**) Mean concentration of ITZ in the medium outside RAW 264.7 cells ± SD (n=3). Statistical analysis in (**A**) was performed using a One-way ANOVA with Fisher's LSD test with ITZ-NS. ****p < 0.0001. Statistical analysis in (**B**) was performed using a One-way ANOVA with Tukey's multiple test with Raw ITZ in Mucus layer.

before macrophage phagocytosis occurred. Some studies have highlighted the significance of ITZ in the mucus and BALF, underscoring the importance of these mechanisms in enhancing ITZ efficacy.[11,12,83,84] Therefore, evasion of phagocytic action and rapid drug delivery into the mucosa are expected to maximize the effectiveness of ITZ.

In-Vivo Pharmacokinetic Studies

A. fumigatus, which causes aspergillosis, thrives in the pulmonary tract. Therefore, direct drug delivery to the lesion sites is crucial for effective treatment. Previous studies have underscored the importance of evaluating the transition and behavior of the ITZ in mucus or BALF, emphasizing the need for adequate drug distribution not only in blood and lung tissue, but also in BALF.[85,86] Pharmacokinetic studies were conducted following a single oral dose of raw ITZ (10 mg/kg) and the intratracheal administration of ITZ in different formulations (JM, NIM-1, NIM-4, and NIM-6) at the same dose. The bioavailability of orally administered ITZ and JM were relatively similar, as shown in Figure 6A. However, the NIM-4 and NIM-6 formulations exhibited slightly increased Cmax and AUC values compared to oral administration, with minimal differences between the two formulations (Table 3 and Figure 6B). These enhancements in plasma drug concentrations may be attributed to the rapid mucosal transit and evasion of macrophages observed prior in-vitro assessments. Pharmacokinetic analyses of lung tissue and BALF were also performed (Figure 6C–F). While oral administration showed almost no ITZ in the lung tissues and BALF, intratracheal administration of JM enabled the identification of ITZ in both the lung tissue and BALF, validating the rationale for the intrapulmonary administration of ITZ. NIM-1 exhibited a drug transition like JM, but NIM-4 and NIM-6 showed a more than two-fold increase in the distribution of ITZ in the BALF (Figure 6F). The BALF serves as an indicator of the lung cavity, pulmonary mucus layer, and sputum. High drug distribution and retention in the pulmonary mucus layer are crucial for the effectiveness of ITZ against Aspergillosis.[87,88] The results of this in-vivo study were consistent with those of previous in-vitro studies. The NIM-4 and NIM-6 formulations, which effectively dispersed nanoparticles in the mucus layer, showed relatively high AUC values owing to the enhanced absorption and evasion of phagocytosis by the nanoparticles. In addition, by maintaining the characteristics of the nanoparticles in the mucus layer, these formulations resulted in significantly higher concentrations of ITZ in the pulmonary cavity and mucus layers than the NIM-1 formulation. This can have a significant impact on the efficacy against fungi residing in the lungs.

In-Vivo Pharmacodynamics Studies

Effectiveness and Hepatotoxicity

An acute pulmonary infection model caused by *A. fumigatus* was developed to evaluate the in-vivo antifungal efficacy of NIM-6 in vivo. We investigated the efficacy of NIM-6 in a rat model of acute invasive pulmonary *A. fumigatus*.[89,90] The rats were divided into five experimental groups (n=4): no *A. fumigatus* infection group (NC), untreated control group (PC), group treated with raw ITZ at 10 mg/kg orally (PO_Raw ITZ), group treated with ITZ via intratracheal administration of the JM formulation (ITI_JM), and group treated with ITZ via intratracheal administration of the NIM-6 formulation (ITI_NIM-6). As shown in Figure 7, acute invasive pulmonary infection increased *A. fumigatus* in the PC group compared to the NC group, but ITI_NIM-6 significantly decreased acute invasive pulmonary *A. fumigatus* infection compared to the PC group. Notably, 75% of the rats in the ITI_NIM-6 treatment group survived for 14 d post-infection, whereas all rats in the PC group died within 6 d, and those in the oral treatment group died within 12 d (Figure 7A). Figure 7B illustrates the changes in body weight among the groups. The PC group exhibited a statistically significant weight loss compared to other groups, showing approximately 77% of its initial body weight on day 7. In contrast, the orally treated group retained 94% of its initial body weight on day 11, the JM intratracheal administration group reached 100% on day 12, and the NIM-6 intratracheal administration group achieved 102% on day 13. These results indicate that the orally treated group showed a slight trend of weight loss compared to the intra-tracheally treated groups. Figure 7C shows the results of ELISA for serum GM concentrations. GM is a structural component of the cell wall of Aspergillus species and can be used as a symptomatic indicator.[91,92] While serum GM concentrations were significantly increased in the PC-and orally administered groups, they were significantly decreased in the groups treated intratracheally with IT_JM and ITI_NIM-6. Figure 7D shows the plasma levels of ALT and ALP, which are typical hepatotoxicity biomarkers. Azole antifungals are potent inhibitors of the liver cytochrome P450

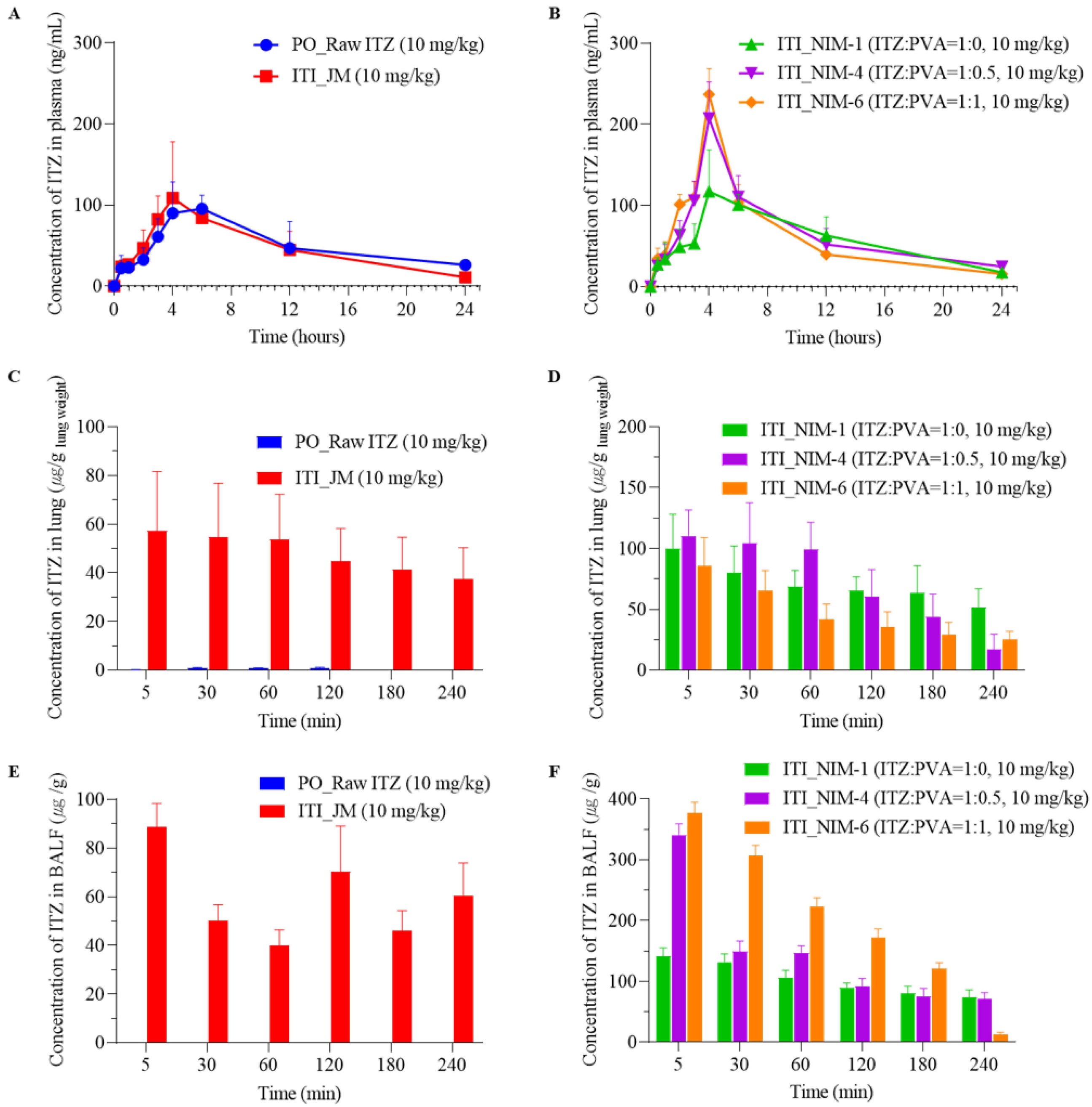

Figure 6 (**A**) Plasma concentration of ITZ after oral administration, (**B**) Plasma concentration of ITZ after ITI administration with NIMs, (**C**) Lung tissue concentration of ITZ after oral administration, (**D**) Lung tissue concentration of ITZ after ITI administration with NIMs, (**E**) BALF concentration of ITZ after oral administration, (**F**) BALF concentration of ITZ after ITI administration with NIMs (mean ± SD, n=5). Statistical analysis in (**F**) was performed using a One-way ANOVA with Tukey's multiple test with NIM-1.

enzymes, potentially leading to increased levels of ALT and ALP, which are indicative of hepatotoxicity.[93] Thus, while the untreated PC group exhibited normal ALT and ALP levels, the orally treated group showed a four-fold increase in ALT and ALP levels compared to the PC group. In contrast, the ITI_JM and ITI_NIM-6 groups exhibited ALT and ALP levels like those of the PC group.[94] This study confirmed the therapeutic efficacy and safety of intratracheally administered ITI_JM and ITI_NIM-6 compared with those of PC or orally administered groups. Intratracheal administration maintained normal hepatotoxicity levels while demonstrating a more potent antifungal effect through galactomannan analysis, thereby showing differences in survival rates and weight maintenance.[95]

Table 3 Pharmacokinetic Profile of ITZ in Plasma After Oral and Inhale Administration With JM, NIM-1, NIM-4, and NIM-6 (Mean ± SD, n=6)

Parameters	Raw ITZ (10 mg/kg) Per oral (P.O.)	JM (10 mg/kg) Intratracheal Installation (ITI)	NIM-1 (ITZ:PVA =1:0,10 mg/kg) Intratracheal Installation (ITI)	NIM-4 (ITZ:PVA =1:0.5,10 mg/kg) Intratracheal Installation (ITI)	NIM-6 (ITZ:PVA =1:1,10 mg/kg) Intratracheal Installation (ITI)
T_{max} (min)	360	240	240	240	240
C_{max} (ng·mL^{-1})	95.5 ± 16.4	108.6 ± 69.3	117.3 ± 51.0	207.5 ± 44.8	237.0 ± 31.7
$AUC_{0\text{-}24h}$ (ng·min·mL^{-1})	396.8 ± 49.2	428.4 ± 60.7	461.5 ± 68.1	623.9 ± 79.2	681.4 ± 65.1
$T_{1/2}$ (min)	936.7	602.6	677.1	630.2	546.6

Pulmonary Fungal Burden

To determine whether NIM-6 effectively inhibited the penetration of *A. fumigatus* into the BALF and lung tissue, CFU analysis was conducted.[96,97] When fungal suppression was assessed by CFU determination, the untreated control group (PC) showed the highest CFU values. However, the CFU values were significantly decreased in the treated group and observed visually (Figure 8A and B). Notably, in Aiv and Biv, the fungal growth area was significantly reduced compared to the other groups. As confirmed in the pharmacokinetic studies, the ITI_NIM-6 group exhibited a consistently higher ITZ concentration in BALF compared to the other groups. Figure 8C illustrates the quantitative CFU in the BALF, and Figure 8D presents the quantitative CFU in the lung tissue. The PC group showed significantly higher values in both the BALF and lung tissues. More specifically, the CFU counts in BALF for the PC, PO_Raw ITZ,

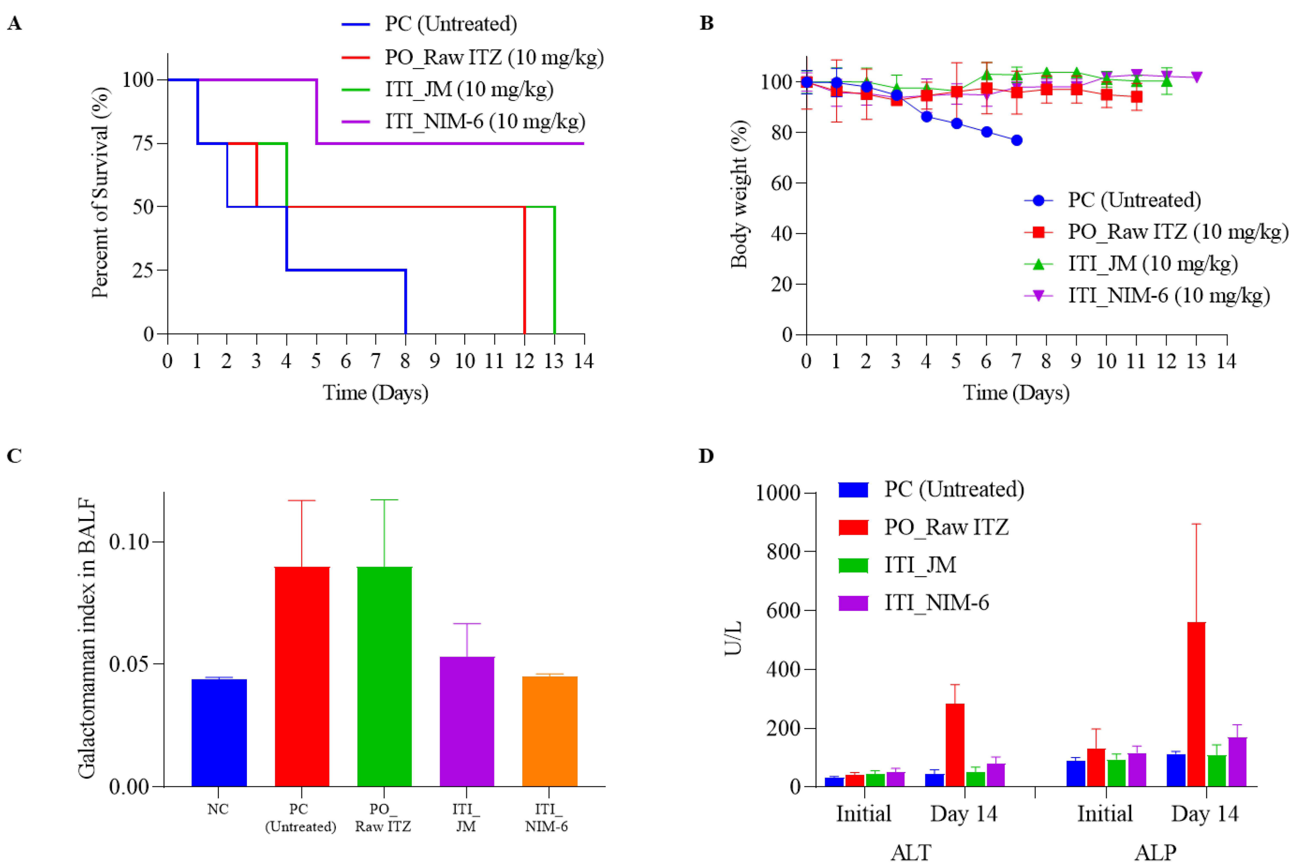

Figure 7 Pharmacodynamic parameters following NIM administration in SD rats infected with *A. fumigatus*; (**A**) survival rate, (**B**) body weight changes, (**C**) galactomannan index in BALF, and (**D**) plasma levels of ALT and ALP. Statistical analyses in (**C**), (D) were performed using a One-way ANOVA with Dunnett's test with PC. Statistical analysis in (**C**) was performed using a One-way ANOVA with Dunnett's test with PO_Raw ITZ.

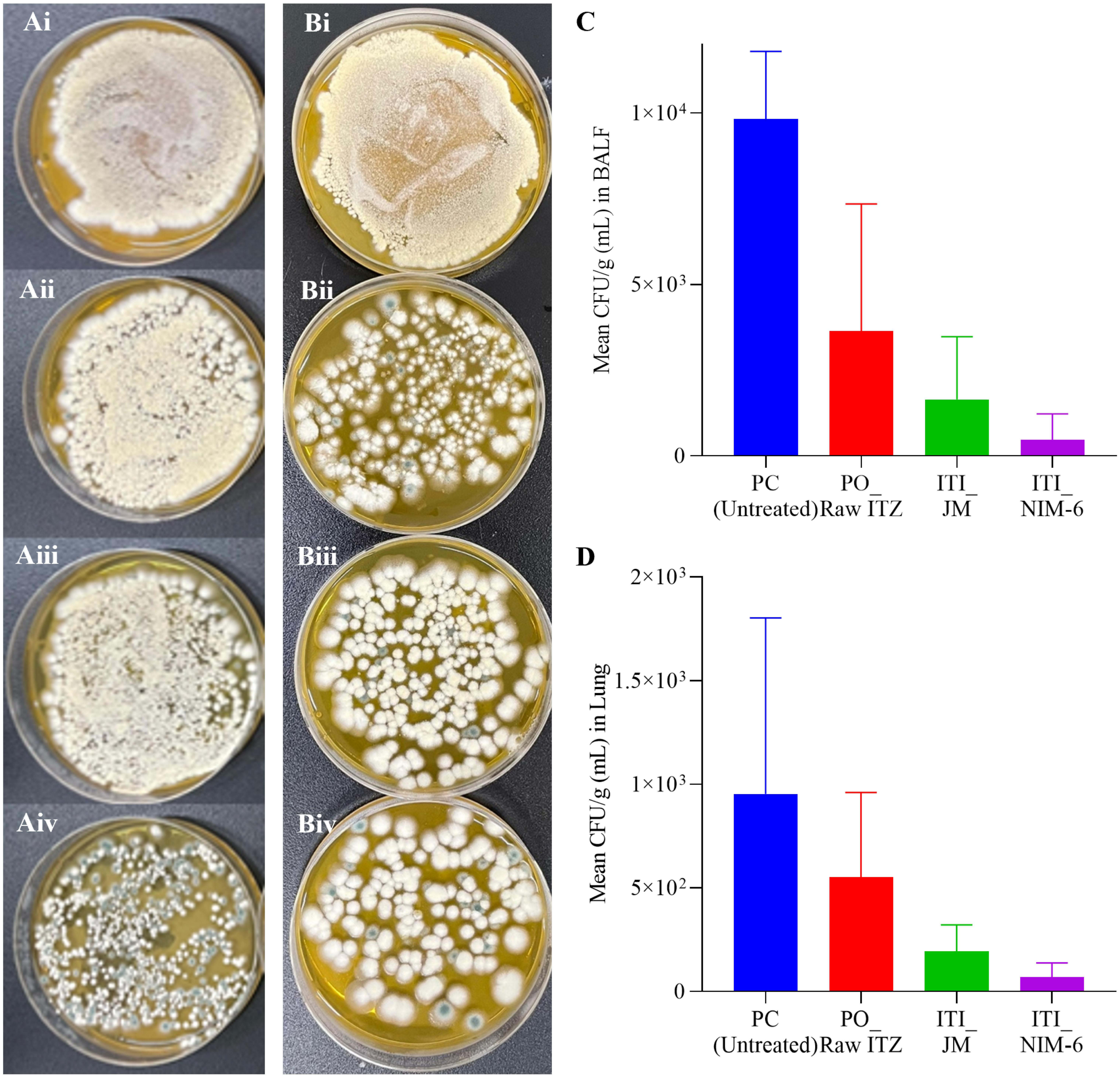

Figure 8 (**A**) Images of fungal cultures obtained from the BALF of SD rats infected with *A. fumigatus*; (Ai) is PC (Untreated), (Aii) is PO_Raw ITZ, (Aiii) is ITI_JM, and (Aiv) is ITI_NIM-6. (**B**) Images of fungal cultures obtained from lung tissues of SD rats infected with *A. fumigatus*; (Bi) is PC (Untreated), (Bii) is PO_Raw ITZ, (Biii) is ITI_JM, and (Biv) is ITI_NIM-6. (**C**) Quantitative analysis of *A. fumigatus* CFU in BALF. (D) in lung tissues (mean ± SD, n=4). *A. fumigatus* from all images were incubated at the same dilution. Statistical analyses in (**C**), (**D**) were performed using a One-way ANOVA with Dunnett's test with PC.

ITI_JM, and ITI_NIM-6 groups were 9817, 3638, 1642, and 465 CFU/g(mL), respectively (Figure 8C), and in lung tissue, they were 953, 552, 193, and 69 CFU/g(mL), respectively (Figure 8D). This study presents an endpoint evaluation of the studies. The NIM-6 formulation, which effectively dispersed nanoparticles in the mucus layer while maintaining their characteristics upon reaching the lungs, facilitated rapid absorption while evading phagocytosis, thus allowing them to remain in the pulmonary cavity and lung tissue. This is believed to effectively reduce the number of fungi present in the lungs and positively affect the survival rates.

Histopathology of Lung

These results demonstrated that NIM-6 enhanced survival rates, reduced symptomatic indicators, and decreased lesion sites in *A. fumigatus* infection model. However, these studies did not elucidate the pathological mechanisms of action of

NIM-6 in *A. fumigatus* infection model. To investigate this further, lung tissues and serum were collected from the *A. fumigatus* infection model. H&E staining was used to visualize the bronchial and alveolar structures of lung tissues, as depicted in Figure 9A and B. The NC group showed intact structures with no evidence of edema or hemorrhage in the lungs. Although direct observation of *A. fumigatus* hyphae was not possible by H&E staining of the PC-and orally treated

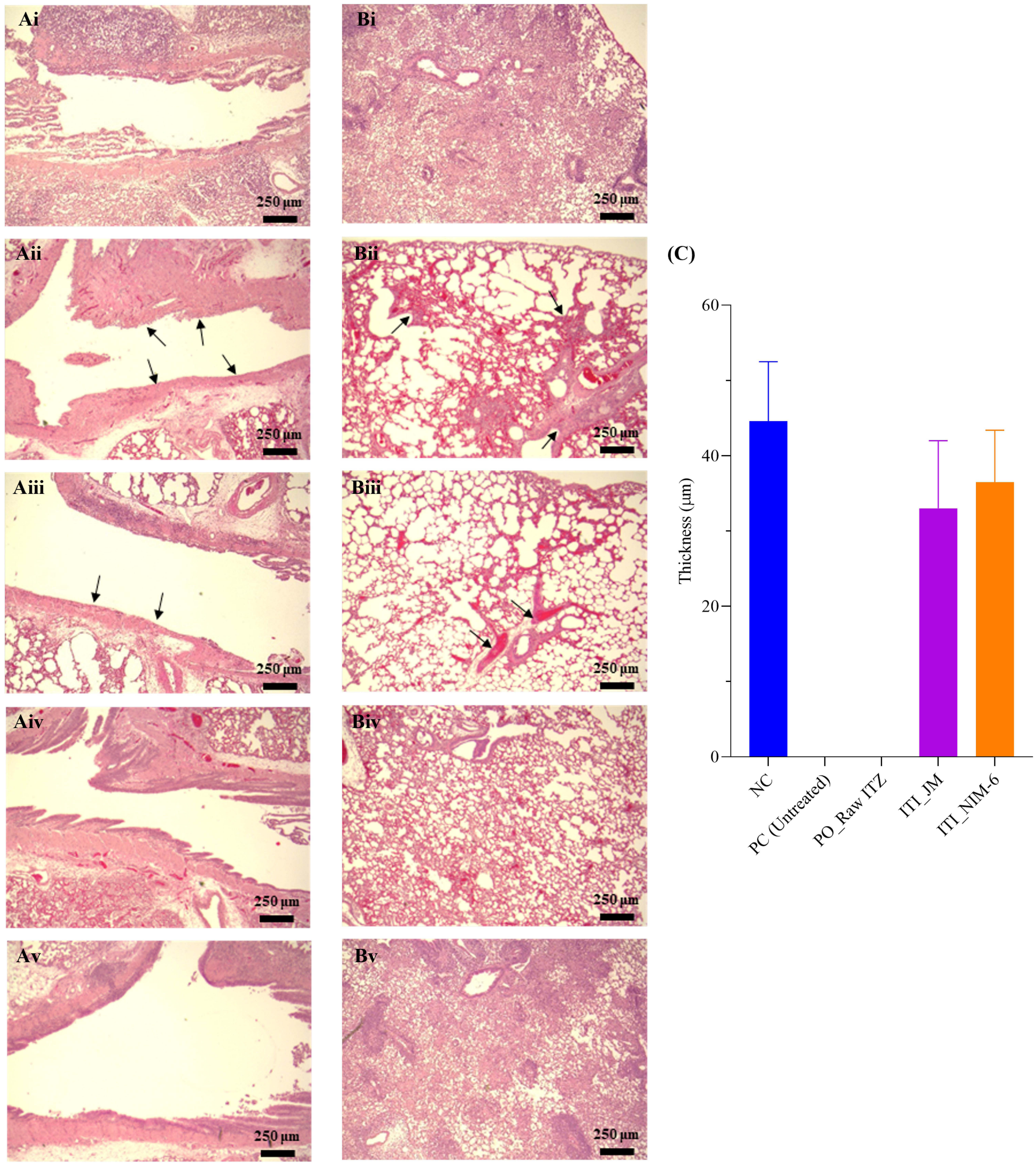

Figure 9 (**A**) Primary bronchus stained with hematoxylin and eosin (H&E) observed under a microscope, magnification 400×; (Ai) Negative control (NC), (Aii) Positive control (PC), (Aiii) PO_Raw ITZ, (Aiv) ITI_JM, (Av) ITI_NIM-6. (**B**) Alveoli stained with hematoxylin and eosin (H&E) observed under a microscope, magnification 400×; (Bi) Negative control (NC), (Bii) Positive control (PC), (Biii) PO_Raw ITZ, (Biv) ITI_JM, (Bv) ITI_NIM-6. (**C**) Measurement of bronchial epithelial cell thickness (mean ± SD, n=10).

groups, lesions within the bronchi and alveoli were observed. Severe damage and loss of bronchial epithelial cells were noted in both the PC and ITZ MP_PO groups, along with hemorrhage (indicated by black arrows in Figure 9A and B).[98] Figure 9C shows the measurement and quantification of the thickness of the epithelial cell layer within the bronchi.[99] The epithelial cell layer was eradicated or undetectable in the PC and PO_Raw ITZ groups. Both the ITI_JM and ITI_NIM-6 groups exhibited similar structures and thicknesses of primary bronchial epithelial cells as those observed in the NC group. These histopathological findings were consistent with the survival data, symptomatic indicators, and CFU data, indicating less invasive disease and vascular invasion in the aerosolized groups, resulting in improved survival rates.[100] However, we emphasize once again that the histopathological findings, along with symptomatic indicators and CFU data in this study, were derived from experiments conducted in SD rats. Therefore, further investigations are required to determine whether absorption and pathological mechanisms in humans exhibit similar behavior.

Conclusion

In conclusion, the inhalable ITZ-NIM formulation was optimized using a spray drying method with adjusted polymer and surfactant concentrations. This formulation achieved uniform fine particle dispersion without altering ITZ crystallinity or molecular structure, as confirmed by stable 2θ peaks and FT-IR spectra. A reduced enthalpy peak suggested partial amorphization around the drug particles. The appropriate blend of an insoluble drug and hydrophilic polymer improved particle solubility and local therapeutic efficiency, resulting in superior aerosol performance. The NIM-4 and NIM-6 formulations, which have a higher hydrophilic polymer content, exhibited higher drug concentrations in the mucus layer and demonstrated resistance to mucociliary clearance and alveolar macrophage phagocytosis. Analysis of BALF, representing the mucosal or alveolar compartments, revealed higher drug residues in formulations with higher hydrophilic polymer content. For pulmonary infections such as aspergillosis, effective drug delivery to target sites while avoiding pulmonary epithelial and alveolar actions has proven to be highly effective and safe.

Furthermore, drug movement and retention within the bronchial lumen or epithelium are more critical for treating lung infections caused by *A. fumigatus* than systemic absorption or drug translocation into the pulmonary tissues. Specifically, the NIM-6 formulation significantly increases drug penetration into the bronchial lumen or epithelium of rats, thereby improving infection indicators, pathological factors, and survival rates, while substantially reducing antifungal toxicity.[101] These results suggest that NIM-6 is a promising novel antifungal formulation with reduced side effects and improved ITZ efficacy.

Data Sharing Statement

The data that support the findings of this study are available from the corresponding author, Professor Chun-Woong Park, upon reasonable request.

Funding

This work was supported by the National Research Foundation of Korea Grant funded by the Korean Government (NRF-2021R1A2C4002746). Additionally, this research was supported by a grant of the Korea Health Technology R&D Project through the Korea Health Industry Development Institute (KHIDI), funded by the Ministry of Health & Welfare, Republic of Korea (grant number: RS-2024-00335798). Furthermore, this work was supported by Chungbuk National University BK21 program (2024).

Disclosure

The authors report no conflicts of interest in this work.

References

1. Denning DW. Invasive aspergillosis. *Clin Infect Dis*. 1998;26:781–803. doi:10.1086/513943
2. McNeil MM, Nash SL, Hajjeh RA, et al. Trends in mortality due to invasive mycotic diseases in the United States, 1980–1997. *Clin Infect Dis*. 2001;33:641–647. doi:10.1086/322606

3. Hope WW, Billaud EM, Lestner J, et al. Therapeutic drug monitoring for triazoles. *Curr Opin Infect Dis*. 2008;21:580–586. doi:10.1097/QCO.0b013e3283184611
4. Coronel B, Levron JC, Van Devenne DDA, et al. Itraconazole lung concentrations in haematological patients. *Mycoses*. 2000;43:125–127. doi:10.1046/j.1439-0507.2000.00565.x
5. Camuset J, Nunes H, Dombret M-C, et al. Treatment of chronic pulmonary aspergillosis by voriconazole in nonimmunocompromised patients. *Chest*. 2007;131:1435–1441. doi:10.1378/chest.06-2441
6. Kanafani ZA, Perfect JR. Resistance to antifungal agents: mechanisms and clinical impact. *Clin Infect Dis*. 2008;46:120–128. doi:10.1086/524071
7. Merlos R, Amighi K, Wauthoz N. Recent developments in inhaled triazoles against invasive pulmonary Aspergillosis. *Curr Fungal Infect Rep*. 2014;8:331–342.
8. Peyton L, Gallagher S, Hashemzadeh M. Triazole antifungals: a review. *Drugs Today*. 2015;51:705–718. doi:10.1358/dot.2015.51.12.2421058
9. Zhang J, Liu Y, Nie X, et al. Trough concentration of itraconazole and its relationship with efficacy and safety: a systematic review and meta-analysis. *Infect Drug Resist*. 2018;11:1283–1297. doi:10.2147/IDR.S170706
10. Cowley AC, Thornton DJ, Denning DW, et al. Aspergillosis and the role of mucins in cystic fibrosis. *Pediatr Pulmonol*. 2017;52:548–555. doi:10.1002/ppul.23618
11. Chabi M, Goracci A, Roche N, et al. Pulmonary aspergillosis. *Diagn Interv Imaging*. 2015;96:435–442. doi:10.1016/j.diii.2015.01.005
12. Phuyal S, Garg MK, Agarwal R, et al. High-attenuation mucus impaction in patients with allergic bronchopulmonary aspergillosis: objective criteria on high-resolution computed tomography and correlation with serologic parameters. *Curr Probl Diagn Radiol*. 2016;45:168–173. doi:10.1067/j.cpradiol.2015.07.006
13. Gaikwad SS, Pathare SR, More MA, et al. Dry powder inhaler with the technical and practical obstacles, and forthcoming platform strategies. *J Control Release*. 2023;355:292–311. doi:10.1016/j.jconrel.2023.01.083
14. Barrons R, Pegram A, Borries A. Inhaler device selection: special considerations in elderly patients with chronic obstructive pulmonary disease. *Am J Health Syst Pharm*. 2011;68:1221–1232. doi:10.2146/ajhp100452
15. Hickey AJ. Dry powder inhalers: an overview. *J Aerosol Med Pulm Drug Deliv*. 2023;36:316–323. doi:10.1089/jamp.2023.29104.ajh
16. Thakkar V, Pandey E, Pandya T, et al. Formulation of dry powder inhaler of anti-tuberculous drugs using spray drying technique and optimization using 23 level factorial design approach. *Curr Drug Ther*. 2019;14:239–260. doi:10.2174/1574885514666190104114209
17. Rattanupatam T, Srichana T. Budesonide dry powder for inhalation: effects of leucine and mannitol on the efficiency of delivery. *Drug Delivery*. 2014;21:397–405. doi:10.3109/10717544.2013.868555
18. Labiris NR, Dolovich MB. Pulmonary drug delivery. Part I: physiological factors affecting therapeutic effectiveness of aerosolized medications. *Br J Clin Pharmacol*. 2003;56:588–599. doi:10.1046/j.1365-2125.2003.01892.x
19. Karner S, Maier M, Littringer E, et al. Surface roughness effects on the tribo-charging and mixing homogeneity of adhesive mixtures used in dry powder inhalers. *Powder Technol*. 2014;264:544–549.
20. Janssen WJ, Stefanski AL, Bochner BS, et al. Control of lung defence by mucins and macrophages: ancient defence mechanisms with modern functions. *Eur Respir J*. 2016;48:1201–1214. doi:10.1183/13993003.00120-2015
21. Mehta PP, Dhapte-Pawar V. *Pulmonary Drug Delivery Systems: Material and Technological Advances*. Springer; 2023.
22. Liu D, Long M, Gao L, et al. Nanomedicines targeting respiratory injuries for pulmonary disease management. *Adv Funct Mater*. 2022;32:2112258.
23. Cappa V, Marcon A, Di Gennaro G, et al. Health-related quality of life varies in different respiratory disorders: a multi-case control population based study. *BMC Pulm Med*. 2019;19:1–8. doi:10.1186/s12890-019-0796-8
24. Torge A, Grützmacher P, Mücklich F, et al. The influence of mannitol on morphology and disintegration of spray-dried nano-embedded microparticles. *Eur J Pharm Sci*. 2017;104:171–179. doi:10.1016/j.ejps.2017.04.003
25. Carrasco-Esteban E, Domínguez-Rullán JA, Barrionuevo-Castillo P, et al. Current role of nanoparticles in the treatment of lung cancer. *J Clin Trans Res*. 2021;7:140.
26. Carvalho TC, Peters JI, Williams RO. Influence of particle size on regional lung deposition–what evidence is there? *Int J Pharm*. 2011;406:1–10. doi:10.1016/j.ijpharm.2010.12.040
27. Kho K, Hadinoto K. Dry powder inhaler delivery of amorphous drug nanoparticles: effects of the lactose carrier particle shape and size. *Powder Technol*. 2013;233:303–311. doi:10.1016/j.powtec.2012.09.023
28. Forest V, Pourchez J. Nano-delivery to the lung-by inhalation or other routes and why nano when micro is largely sufficient? *Adv Drug Deliv Rev*. 2022;183:114173. doi:10.1016/j.addr.2022.114173
29. Hoppentocht M, Hagedoorn P, Frijlink H, et al. Technological and practical challenges of dry powder inhalers and formulations. *Adv Drug Deliv Rev*. 2014;75:18–31. doi:10.1016/j.addr.2014.04.004
30. Vehring R, Foss WR, Lechuga-Ballesteros D. Particle formation in spray drying. *J Aerosol Sci*. 2007;38:728–746. doi:10.1016/j.jaerosci.2007.04.005
31. Vehring R. Pharmaceutical particle engineering via spray drying. *Pharma Res*. 2008;25:999–1022. doi:10.1007/s11095-007-9475-1
32. Scherließ R, Bock S, Bungert N, et al. Particle engineering in dry powders for inhalation. *Eur J Pharm Sci*. 2022;172:106158. doi:10.1016/j.ejps.2022.106158
33. Weers J, Tarara T. The PulmoSphere™ platform for pulmonary drug delivery. *Ther Deliv*. 2014;5:277–295. doi:10.4155/tde.14.3
34. Li X, Vogt FG, Hayes D, et al. Design, characterization, and aerosol dispersion performance modeling of advanced co-spray dried antibiotics with mannitol as respirable microparticles/nanoparticles for targeted pulmonary delivery as dry powder inhalers. *J Pharm Sci*. 2014;103:2937–2949. doi:10.1002/jps.23955
35. Alhajj N, Zakaria Z, Naharudin I, et al. Critical physicochemical attributes of chitosan nanoparticles admixed lactose-PEG 3000 microparticles in pulmonary inhalation. *Asian J Pharm Sci*. 2020;15:374–384. doi:10.1016/j.ajps.2019.02.001
36. Licciardi M, Di Stefano M, Craparo EF, et al. PHEA-graft-polybutylmethacrylate copolymer microparticles for delivery of hydrophobic drugs. *Int J Pharm*. 2012;433:16–24. doi:10.1016/j.ijpharm.2012.04.052

37. Vijayaraghavan M, Stolnik S, Howdle SM, et al. Suitability of polymer materials for production of pulmonary microparticles using a PGSS supercritical fluid technique: preparation of microparticles using PEG, fatty acids and physical or chemicals blends of PEG and fatty acids. *Int J Pharm*. 2013;441:580–588. doi:10.1016/j.ijpharm.2012.10.040
38. Wang M-Y, YuT Chang Y-T. New method for preparing more stable microcapsules for the entrapment of genetically engineered cells. *Artif Cells Blood Substit Biotechnol*. 2005;33:257–269. doi:10.1081/BIO-200066606
39. Beck-Broichsitter M, Samsonova O, Nguyen J, et al. Influence of amine-modified poly (vinyl alcohol) s on vibrating-membrane nebulizer performance and lung toxicity. *Eur J Pharm Sci*. 2016;86:34–40. doi:10.1016/j.ejps.2016.02.023
40. Murata M, Nakano K, Tahara K, et al. Pulmonary delivery of elcatonin using surface-modified liposomes to improve systemic absorption: polyvinyl alcohol with a hydrophobic anchor and chitosan oligosaccharide as effective surface modifiers. *Eur J Pharm Biopharm*. 2012;80:340–346. doi:10.1016/j.ejpb.2011.10.011
41. Popov A, Enlow E, Bourassa J, et al. Mucus-penetrating nanoparticles made with "mucoadhesive" poly (vinyl alcohol). *Nanomed Nanotechnol Biol Med*. 2016;12:1863–1871. doi:10.1016/j.nano.2016.04.006
42. Yamamoto A, Yamada K, Muramatsu H, et al. Control of pulmonary absorption of water-soluble compounds by various viscous vehicles. *Int J Pharm*. 2004;282:141–149. doi:10.1016/j.ijpharm.2004.06.008
43. Saigal A, Ng WK, Tan RB, et al. Development of controlled release inhalable polymeric microspheres for treatment of pulmonary hypertension. *Int J Pharm*. 2013;450:114–122. doi:10.1016/j.ijpharm.2013.04.011
44. Chen Z, Wu W, Lu Y. What is the future for nanocrystal-based drug-delivery systems? *Ther Deliv*. 2020;11:225–229. doi:10.4155/tde-2020-0016
45. Huang Z, Lin L, McGoverin C, et al. Dry powder inhaler formulations of poorly water-soluble itraconazole: a balance between in-vitro dissolution and in-vivo distribution is necessary. *Int J Pharm*. 2018;551:103–110. doi:10.1016/j.ijpharm.2018.09.018
46. Moss OR. Simulants of lung interstitial fluid. *Health Phys*. 1979;36:447–448.
47. Valo H, Kovalainen M, Laaksonen P, et al. Immobilization of protein-coated drug nanoparticles in nanofibrillar cellulose matrices—enhanced stability and release. *J Control Release*. 2011;156:390–397. doi:10.1016/j.jconrel.2011.07.016
48. Philippe B, Ibrahim-Granet O, Prevost M, et al. Killing of *Aspergillus fumigatus* by alveolar macrophages is mediated by reactive oxidant intermediates. *Infect Immun*. 2003;71:3034–3042. doi:10.1128/IAI.71.6.3034-3042.2003
49. Mitsutake K, Kohno S, Miyazaki T, et al. Detection of (1–3)-β-D-glucan in a rat model of aspergillosis. *J Clin Lab Anal*. 1995;9:119–122. doi:10.1002/jcla.1860090208
50. Miyazaki HM, Kohno S, Miyazaki Y, et al. Efficacy of intravenous itraconazole against experimental pulmonary aspergillosis. *Antimicrob Agents Chemother*. 1993;37:2762–2765. doi:10.1128/AAC.37.12.2762
51. Zhong J, Huang W, Deng Q, et al. Inhibition of TREM-1 and Dectin-1 alleviates the severity of fungal keratitis by modulating innate immune responses. *PLoS One*. 2016;11:e0150114.
52. Ren S, Zhang F, Li C, et al. Selection of housekeeping genes for use in quantitative reverse transcription PCR assays on the murine cornea. *mol Vis*. 2010;16:1076.
53. Desoubeaux G, Chandenier J. A nebulized intra-tracheal rat model of invasive pulmonary aspergillosis. In:*Host-Fungus Interactions: Methods Protocols*. 2012:511–518.
54. Prüfer S, Weber M, Stein P, et al. Oxidative burst and neutrophil elastase contribute to clearance of *Aspergillus fumigatus* pneumonia in mice. *Immunobiology*. 2014;219:87–96. doi:10.1016/j.imbio.2013.08.010
55. Pfeiffer CD, Fine JP, Safdar N. Diagnosis of invasive aspergillosis using a galactomannan assay: a meta-analysis. *Clin Infect Dis*. 2006;42:1417–1727.
56. Mennink-Kersten MA, Donnelly JP, Verweij PE. Detection of circulating galactomannan for the diagnosis and management of invasive aspergillosis. *Lancet Infect Dis*. 2004;4:349–357.
57. Huang X-J, Choi Y-K, Im H-S, et al. Aspartate aminotransferase (AST/GOT) and alanine aminotransferase (ALT/GPT) detection techniques. *Sensors*. 2006;6:756–782.
58. Denning DW, Pleuvry A, Cole DC. Global burden of allergic bronchopulmonary aspergillosis with asthma and its complication chronic pulmonary aspergillosis in adults. *Med Mycol*. 2013;51:361–370. doi:10.3109/13693786.2012.738312
59. Singh G, Imai J, Clemons KV, et al. Efficacy of caspofungin against central nervous system *Aspergillus fumigatus* infection in mice determined by TaqMan PCR and CFU methods. *Antimicrob Agents Chemother*. 2005;49:1369–1376.
60. Zhang X, Zhou Y, Wang G, et al. Co-spray-dried poly-L-lysine with L-leucine as dry powder inhalations for the treatment of pulmonary infection: moisture-resistance and desirable aerosolization performance. *Int J Pharm*. 2022;624:122011.
61. Birchal V, Huang L, Mujumdar A, et al. Spray dryers: modeling and simulation. *Dry Technol*. 2006;24:359–371.
62. Tang P, Chan H-K, Raper JA. Prediction of aerodynamic diameter of particles with rough surfaces. *Powder Technol*. 2004;147:64–78.
63. Alemrayat B, Elrayess MA, Alany RG, et al. Preparation and optimization of monodisperse polymeric microparticles using modified vibrating orifice aerosol generator for controlled delivery of letrozole in breast cancer therapy. *Drug Dev Ind Pharm*. 2018;44(12):1953–1965. doi:10.1080/03639045.2018.1503298
64. Radhakrishnan B, Balerdi G, Cloutet E, et al. Hydroxy and di-hydroxy end-capped polybutadiene as reactive steric stabilizers for the synthesis of polyurethane particles in organic dispersant media. *Macromol Symp*. 2005;229(1):56–65. doi:10.1002/masy.200551107
65. Danaei M, Dehghankhold M, Ataei S, et al. Impact of particle size and polydispersity index on the clinical applications of lipidic nanocarrier systems. *Pharmaceutics*. 2018;10:57. doi:10.3390/pharmaceutics10020057
66. Reshmi C, Sundaran SP, Subija T, et al. "Nano in micro" architecture composite membranes for controlled drug delivery. *Appl Clay Sci*. 2018;166:262–275. doi:10.1016/j.clay.2018.08.015
67. Ramos JJM, Diogo HP. The slow relaxation dynamics in active pharmaceutical ingredients studied by DSC and TSDC: voriconazole, miconazole and itraconazole. *Int J Pharm*. 2016;501:39–48. doi:10.1016/j.ijpharm.2016.01.057
68. Wlodarski K, Zhang F, Liu T, et al. Synergistic effect of polyvinyl alcohol and copovidone in itraconazole amorphous solid dispersions. *Pharma Res*. 2018;35:1–15. doi:10.1007/s11095-017-2313-1
69. Wang X, Michoel A, Van den Mooter G. Study of the phase behavior of polyethylene glycol 6000–itraconazole solid dispersions using DSC. *Int J Pharm*. 2004;272:181–187. doi:10.1016/j.ijpharm.2003.11.026

70. Fernández-Ronco MP, Salvalaglio M, Kluge J, et al. Study of the preparation of amorphous itraconazole formulations. *Cryst Growth Des*. 2015;15:2686–2694.
71. Kumar S, Jog R, Shen J, et al. In vitro and in vivo performance of different sized spray-dried crystalline itraconazole. *J Pharm Sci*. 2015;104:3018–3028. doi:10.1002/jps.24155
72. De Smet L, Saerens L, De Beer T, et al. Formulation of itraconazole nanococrystals and evaluation of their bioavailability in dogs. *Eur J Pharm Biopharm*. 2014;87:107–113. doi:10.1016/j.ejpb.2013.12.016
73. Kawakami K, Sumitani C, Yoshihashi Y, et al. Investigation of the dynamic process during spray-drying to improve aerodynamic performance of inhalation particles. *Int J Pharm*. 2010;390:250–259.
74. Lee H-J, Lee H-G, Kwon Y-B, et al. The role of lactose carrier on the powder behavior and aerodynamic performance of bosentan microparticles for dry powder inhalation. *Eur J Pharm Sci*. 2018;117:279–289. doi:10.1016/j.ejps.2018.03.004
75. Kwon Y-B, Kang J-H, Han C-S, et al. The effect of particle size and surface roughness of spray-dried bosentan microparticles on aerodynamic performance for dry powder inhalation. *Pharmaceutics*. 2020;12:765.
76. Adi S, Adi H, Tang P, et al. Micro-particle corrugation, adhesion and inhalation aerosol efficiency. *Eur J Pharm Sci*. 2008;35:12–18.
77. Musa N, Wong TW. Design of polysaccharidic nano-in-micro soft agglomerates as primary oral drug delivery vehicle for colon-specific targeting. *Carbohydr Polym*. 2020;247:116673. doi:10.1016/j.carbpol.2020.116673
78. Mejias JC. Nano-in-micro multi-stage particles for pulmonary drug delivery; 2019.
79. Chen D, Liu S, Chen D, et al. A two-pronged pulmonary gene delivery strategy: a surface-modified fullerene nanoparticle and a hypotonic vehicle. *Angew Chem Int Ed*. 2021;60:15225–15229. doi:10.1002/anie.202101732
80. Patel B, Gupta N, Ahsan F. Particle engineering to enhance or lessen particle uptake by alveolar macrophages and to influence the therapeutic outcome. *Eur J Pharm Biopharm*. 2015;89:163–174. doi:10.1016/j.ejpb.2014.12.001
81. Chono S, Tanino T, Seki T, et al. Influence of particle size on drug delivery to rat alveolar macrophages following pulmonary administration of ciprofloxacin incorporated into liposomes. *J Drug Target*. 2006;14:557–566. doi:10.1080/10611860600834375
82. Geng Y, Dalhaimer P, Cai S, et al. Shape effects of filaments versus spherical particles in flow and drug delivery. *Nat Nanotechnol*. 2007;2:249–255. doi:10.1038/nnano.2007.70
83. Agarwal R, Gupta D, Aggarwal AN, et al. Clinical significance of hyperattenuating mucoid impaction in allergic bronchopulmonary aspergillosis: an analysis of 155 patients. *Chest*. 2007;132:1183–1190. doi:10.1378/chest.07-0808
84. Franquet T, Muller NL, Giménez A, et al. Spectrum of pulmonary aspergillosis: histologic, clinical, and radiologic findings. *Radiographics*. 2001;21:825–837. doi:10.1148/radiographics.21.4.g01jl03825
85. Duret C, Merlos R, Wauthoz N, et al. Pharmacokinetic evaluation in mice of amorphous itraconazole-based dry powder formulations for inhalation with high bioavailability and extended lung retention. *Eur J Pharm Biopharm*. 2014;86:46–54. doi:10.1016/j.ejpb.2013.03.005
86. Izumikawa K, Yamamoto Y, Mihara T, et al. Bronchoalveolar lavage galactomannan for the diagnosis of chronic pulmonary aspergillosis. *Med Mycol*. 2012;50:811–817. doi:10.3109/13693786.2012.682228
87. Ye F, Zeng P, Li Z, et al. Detection of Aspergillus DNA in BALF by real-time PCR and galactomannan antigen for the early diagnosis of chronic pulmonary aspergillosis. *Ann Clin Lab Sci*. 2021;51:698–704.
88. Sehgal IS, Dhooria S, Choudhary H, et al. Utility of serum and bronchoalveolar lavage fluid galactomannan in diagnosis of chronic pulmonary aspergillosis. *J Clin Microbiol*. 2019;57. doi:10.1128/jcm.01821-18
89. Yan Y, Zhao Z, Wan H, et al. A novel fungus concentration-dependent rat model for acute invasive fungal rhinosinusitis: an experimental study. *BMC Infect Dis*. 2014;14:1–11. doi:10.1186/s12879-014-0713-y
90. Ahmad S, Al-Shaikh AA, Khan Z. Development of a novel inhalational model of invasive pulmonary aspergillosis in rats and comparative evaluation of three biomarkers for its diagnosis. *PLoS One*. 2014;9:e100524. doi:10.1371/journal.pone.0100524
91. Park SY, Lee S-O, Choi S-H, et al. Aspergillus galactomannan antigen assay in bronchoalveolar lavage fluid for diagnosis of invasive pulmonary aspergillosis. *J Infect*. 2010;61:492–498. doi:10.1016/j.jinf.2010.08.014
92. Francesconi A, Kasai M, Petraitiene R, et al. Characterization and comparison of galactomannan enzyme immunoassay and quantitative real-time PCR assay for detection of *Aspergillus fumigatus* in bronchoalveolar lavage fluid from experimental invasive pulmonary aspergillosis. *J Clin Microbiol*. 2006;44:2475–2480. doi:10.1128/JCM.02693-05
93. Somchit N, Norshahida A, Hasiah A, et al. Hepatotoxicity induced by antifungal drugs itraconazole and fluconazole in rats: a comparative in vivo study. *Hum Exp Toxicol*. 2004;23:519–525. doi:10.1191/0960327104ht479oa
94. Kemeir ME-HA. Hepatotoxic effect of itraconazole in experimental rats. *Am J Anim Vet Sci*. 2014;9:46–52. doi:10.3844/ajavsp.2014.46.52
95. Khoza S, Moyo I, Ncube D. Comparative hepatotoxicity of fluconazole, ketoconazole, itraconazole, terbinafine, and griseofulvin in rats. *J Toxicol*. 2017;2017:1–9. doi:10.1155/2017/6746989
96. Colley T, Sehra G, Chowdhary A, et al. In vitro and in vivo efficacy of a novel and long-acting fungicidal azole, PC1244, on *Aspergillus fumigatus* infection. *Antimicrob Agents Chemother*. 2018;62. doi:10.1128/aac.01941-17
97. Nayak AP, Croston TL, Lemons AR, et al. *Aspergillus fumigatus* viability drives allergic responses to inhaled conidia. *Ann Allergy Asthma Immunol*. 2018;121:200–210.e2. doi:10.1016/j.anai.2018.04.008
98. Shibuya K, Hasegawa C, Hamatani S, et al. Pathophysiology of pulmonary aspergillosis. *J Infect Chemother*. 2004;10:138–145. doi:10.1007/s10156-004-0315-5
99. Muldoon EG, Sharman A, Page I, et al. Aspergillus nodules; another presentation of chronic pulmonary aspergillosis. *BMC Pulm Med*. 2016;16:1–9. doi:10.1186/s12890-016-0276-3
100. Tochigi N, Okubo Y, Ando T, et al. Histopathological implications of Aspergillus infection in lung. *Mediators Inflammation*. 2013;2013:1–8. doi:10.1155/2013/809798
101. Zhou Z-X, Yin X-D, Zhang Y, et al. Antifungal drugs and drug-induced liver injury: a real-world study leveraging the FDA adverse event reporting system database. *Front Pharmacol*. 2022;13:891336. doi:10.3389/fphar.2022.891336